

Kinematics and Dynamics for Computer Animation

H. Ruder, T. Ertl, K. Gruber, M. Günther, F. Hospach,
M. Ruder, J. Subke, K. Widmayer

1 Introduction

In the first phase of computer animation the traditional techniques of animation were brought to the computer resulting in computer animated films where the keyframes were linked by image-based and parametric interpolation. Especially when trying to compute aesthetic human movement it soon became obvious that a more realistic computer animation has to take into account the basic physical properties of the objects and the fundamental physical principles that govern their movement. In algorithmic animation the evolution of the state of a system of objects is not determined by interpolation, but by physical laws given either as algebraic formulae in the simple case or more complicated as set of coupled nonlinear differential equations. In kinematic animation the objects are moved according to a set of given equations for the velocities or the accelerations at certain points of the objects. This procedure results in a realistic animation only if the prescribed velocities and accelerations were derived from a complete dynamic physical model. Therefore, the most general approach for generating physically correct animation sequences is to perform a full dynamical simulation of the given model taking into account all external and internal forces and torques.

However, a complete dynamical simulation of a synthetic human actor in realtime (which requires much more than just the correct movement of the skeleton) is far beyond the capabilities of modern computers and simulation software. Only rigid objects with a few degrees of freedom or very simple elastic models can be treated today and there are many unresolved questions of how to control the internal torques in order to get the desired motion. Thus, generating appealing animation today still requires a lot of heuristics, experimental data and a combination of keyframing, kinematic and dynamic algorithms. Nevertheless, the importance of dynamic modelling will continue to grow since it is the only method which guarantees the equivalence of modelling and animation, which means that the temporal behaviour of physical based objects is bound up in the model itself.

This tutorial will focus on the physical principles of kinematics and dynamics. After explaining the basic equations for point masses and rigid bodies a new approach for the dynamic simulation of multi-linked models with wobbling mass is presented, which has led to new insight in the field of biomechanics, but which has not been used in computer animation so far.

2 Kinematic fundamentals

We will briefly review the kinematics of point masses and extended rigid bodies, which is just the geometrical description of the motion. Those motions take place in a three-dimensional coordinate system, where points in space are denoted by the position vector pointing from the origin of the coordinate system to the respective end points (cf. Fig. 2.1). Whenever it is convenient, we leave the coordinate-free formulation and switch to cartesian, cylindrical or spherical coordinates. Besides the space coordinates \mathbf{r} which we are completely free to choose, kinematics introduces a time coordinate t which can be looked at as the independent variable.

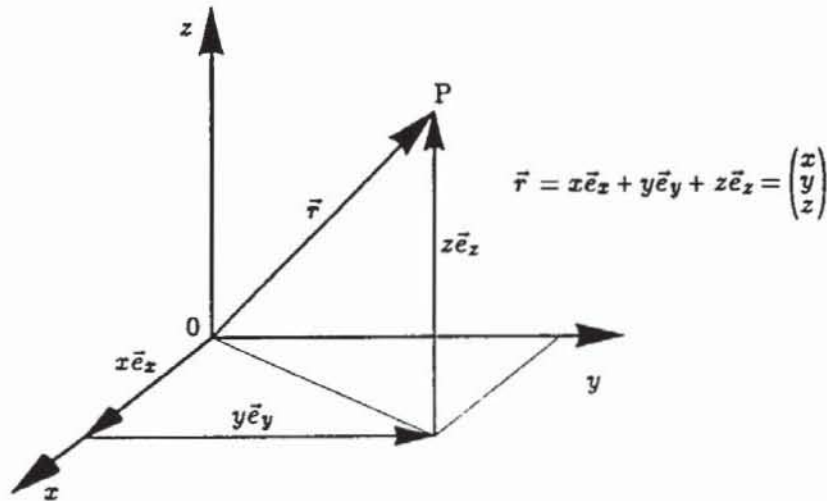


Fig. 2.1. The position vector \mathbf{r} of a point P and its coordinates in a cartesian coordinate system.

2.1 Kinematics of a point mass

When describing the motion of an object where the size of the object is negligible compared to the distances covered and where rotations and deformations are of no interest, the object may be idealized by a mathematical point characterized by a mass. The motion of a point mass is completely described by its trajectory in space, e.g. its position vector $\mathbf{r}(t)$ and its velocity $\mathbf{v}(t)$ at the time t (cf. Fig. 2.2) The velocity is given by

$$\mathbf{v}(t) = \dot{\mathbf{r}}(t) \quad , \quad (2.1)$$

where the time derivative is defined as usual:

$$\dot{\mathbf{r}}(t) = \frac{d\mathbf{r}}{dt} = \lim_{\delta t \rightarrow 0} \frac{\mathbf{r}(t + \delta t) - \mathbf{r}(t)}{\delta t} \quad . \quad (2.2)$$

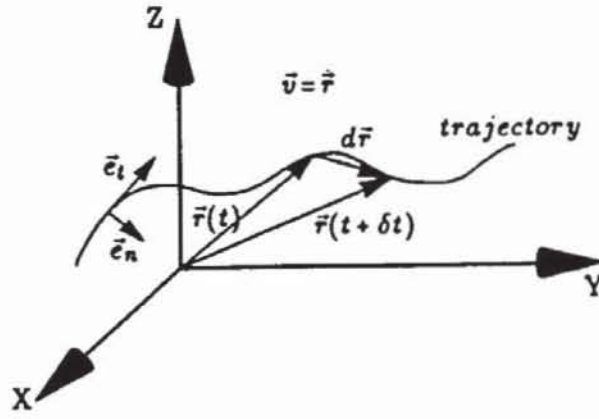


Fig. 2.2. Trajectory of a point mass in space. The unit vector e_t is tangential to the trajectory, whereas the unit vector e_n is perpendicular to the trajectory in the local osculating plane.

The component of the velocity tangential to the trajectory is the absolute value of the velocity v , the component normal to the trajectory is zero

$$v_t = v e_t \quad (2.3a)$$

$$v_n = 0 \quad (2.3b)$$

where e_t denotes the unit vector tangential to the trajectory. Therefore, the length of the path s covered since t_0 is

$$s(t) = \int_{t_0}^t v dt' \quad (2.4)$$

A further important quantity is the acceleration $a(t)$ of the mass point, defined as:

$$a(t) = \dot{v}(t) = \ddot{r}(t) \quad (2.5)$$

Its components tangential and normal to the trajectory are given by

$$a_t = \dot{v} e_t \quad (2.6a)$$

$$a_n = \frac{v^2}{\rho} e_n \quad (2.6b)$$

Here, e_n means the unit vector normal to the trajectory, which lies in the local osculating plane and ρ is the corresponding local curvature radius.

One elementary example is the parabola of a throw in a uniform gravitational field (cf. Fig. 2.3). Using appropriate initial conditions,

$$a = g = -g e_z \quad (2.7a)$$

can be integrated to

$$v(t) = v_0 + g t = v_0 \cos \alpha e_x + (v_0 \sin \alpha - g t) e_z \quad (2.7b)$$

which again can be integrated to

$$r(t) = (v_0 t \cos \alpha + x_0) e_x + (v_0 t \sin \alpha - \frac{1}{2} g t^2 + z_0) e_z \quad (2.7c)$$

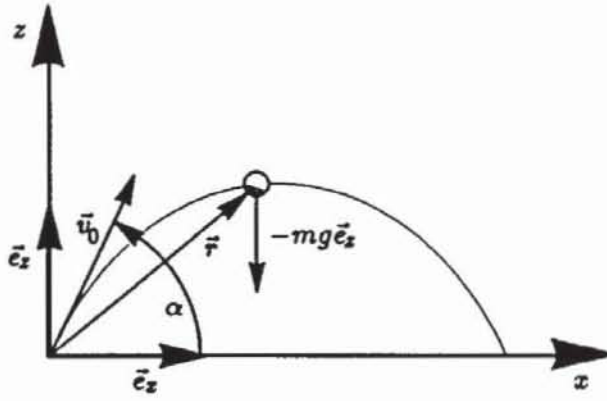


Fig. 2.3. The throw in a uniform gravitational field with initial velocity v_0 and inclination α .

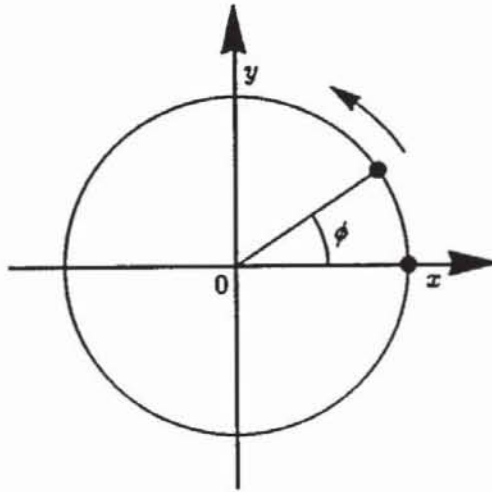


Fig. 2.4. The circular motion with constant angular velocity $\omega = \dot{\phi}$.

This procedure, which derives the motion $\mathbf{r}(t)$ from a given acceleration $\mathbf{a}(t)$ is called *direct kinematics* and results in the well known parabolic path:

$$z = \tan \alpha x - \frac{g}{2v_0^2 \cos^2 \alpha} x^2 \quad \text{with } x_0 = 0, z_0 = 0 \quad . \quad (2.8)$$

In *inverse kinematics* the acceleration $\mathbf{a}(t)$ is derived from the path $\mathbf{r}(t)$ by differentiation like in the example of the circular motion with constant angular velocity $\omega = \frac{\dot{\phi}}{t}$ (cf. Fig. 2.4):

$$\mathbf{r}(t) = r \cos \omega t \mathbf{e}_x + r \sin \omega t \mathbf{e}_y \quad (2.9a)$$

$$\mathbf{v}(t) = \dot{\mathbf{r}}(t) = -\omega r \sin \omega t \mathbf{e}_x + \omega r \cos \omega t \mathbf{e}_y \quad (2.9b)$$

$$\mathbf{a}(t) = \dot{\mathbf{v}}(t) = \ddot{\mathbf{r}}(t) = -\omega^2 \mathbf{r}(t) \quad . \quad (2.9c)$$

The velocity \mathbf{v} is always perpendicular to the position vector \mathbf{r} ($\mathbf{r} \cdot \mathbf{v} = 0$) and the vector of the angular velocity ω can be introduced by $\mathbf{r} \times \mathbf{v}/r^2 = \omega \mathbf{e}_z = \omega$.

More complicated than the circular motion is the motion of the planets around the sun. The three Kepler laws

1. The orbit of each planet is an ellipse with the sun at one focus.
2. The radius vector from the sun to a planet sweeps out equal areas in equal intervals of time.
3. The squares of the periods of revolution of any two planets are proportional to the cubes of the semimajor axes of the respective orbits.

are a purely kinematic description based on observations. They can be used to derive the structure of the gravitational force or vice versa Newton's law of gravitation can be used to derive Kepler's observations .

2.2 Kinematics of a rigid body

In order to uniquely describe the position and the orientation of a rigid body in space six independent coordinates are necessary. Of course, there exist a lot of different possibilities for realization. An appropriate way is to use the three cartesian coordinates of the center of mass x_c, y_c, z_c defined by

$$\mathbf{r}_c = (x_c, y_c, z_c) = \frac{\int_{\text{vol}} \mathbf{r} \rho(x, y, z) dx dy dz}{\int_{\text{vol}} \rho(x, y, z) dx dy dz} \quad (2.10)$$

where $\rho(x, y, z)$ is the mass density, and α, β, γ are the three Eulerian angles for the orientation of a body-fixed coordinate system $\xi\eta\zeta$, whose origin coincides with the center of mass (cf. Fig. 2.5), with respect to the directions of the space-fixed axes $(X), (Y), (Z)$.

The most general motion of the rigid body is the superposition of the velocity of its center of mass $\dot{\mathbf{r}}_c(t) = \mathbf{v}_c$ and a rotation around the center of mass with an angular velocity $\omega(t)$:

$$\dot{\mathbf{r}}(t) = \mathbf{v}_c(t) + \omega(t) \times (\mathbf{r}(t) - \mathbf{r}_c(t)) \quad (2.11)$$

The vector ω of the instantaneous angular velocity can be projected onto the space-fixed axes as well as onto the axes of the body-fixed coordinate system. These components can be expressed by the Eulerian angles and their time derivatives

$$\omega_x = -\dot{\beta} \sin \alpha + \dot{\gamma} \sin \beta \cos \alpha \quad (2.12a)$$

$$\omega_y = \dot{\beta} \cos \alpha + \dot{\gamma} \sin \beta \sin \alpha \quad (2.12b)$$

$$\omega_z = \dot{\alpha} + \dot{\gamma} \cos \beta \quad (2.12c)$$

$$\omega_\xi = -\dot{\alpha} \sin \beta \cos \gamma + \dot{\beta} \sin \gamma \quad (2.13a)$$

$$\omega_\eta = \dot{\alpha} \sin \beta \sin \gamma + \dot{\beta} \cos \gamma \quad (2.13b)$$

$$\omega_\zeta = \dot{\alpha} \cos \beta + \dot{\gamma} \quad (2.13c)$$

An example is the force-free motion of a symmetric top.

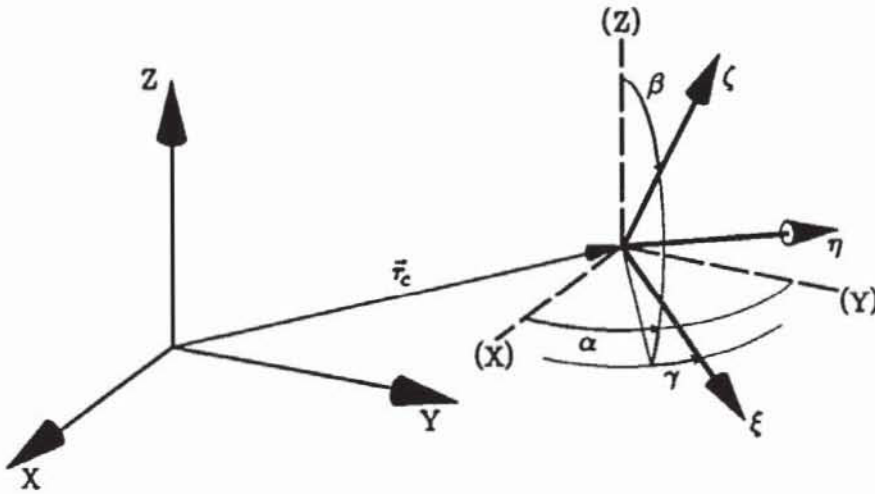


Fig. 2.5. Coordinates for the determination of position and orientation of a rigid body in space. The Euler angle β is the angle between the (Z) - and ζ -axis, the Euler angle α is defined as the angle between the line of intersection of the $(Z)\zeta$ -plane with the $(X)(Y)$ -plane and the (X) -axis, and the Euler angle γ is the angle between the line of intersection of the $(Z)\zeta$ -plane with the $\xi\eta$ -plane and the ξ -axis.

2.3 Kinematics of the special theory of relativity

When computing animation sequences which involve relative motions of the objects or of the observer, usually a Galilei transformation

$$\begin{aligned} x' &= x - Vt \\ y' &= y \\ z' &= z \\ t' &= t \end{aligned} \quad (2.14)$$

is applied to transform from a coordinate system XYZ to a system $X'Y'Z'$ moving relative to each other in X (and X') direction with the velocity V (cf. Fig. 2.6). This is a very good approximation for terrestrial scenarios with relative velocities much smaller than the velocity of light. The correct space-time structure of our physically real world, however, is much more complex and not imaginable for us. This very strange structure is revealed only at velocities, which approach the velocity of light. Therefore, the correct relativistic behaviour must be taken into account for the animation of extraterrestrial scenes in astrophysical simulations and, of course, in a correct modelling of science fiction.

As the essential step in the transition from non relativistic to relativistic kinematics the Galilei transformation (2.14) has to be replaced by the Lorentz transformation

$$\begin{aligned} x' &= \frac{x - Vt}{\sqrt{1 - (\frac{V}{c})^2}} \\ y' &= y \\ z' &= z \\ t' &= \frac{t - (\frac{V}{c^2})x}{\sqrt{1 - (\frac{V}{c})^2}} \end{aligned} \quad (2.15)$$

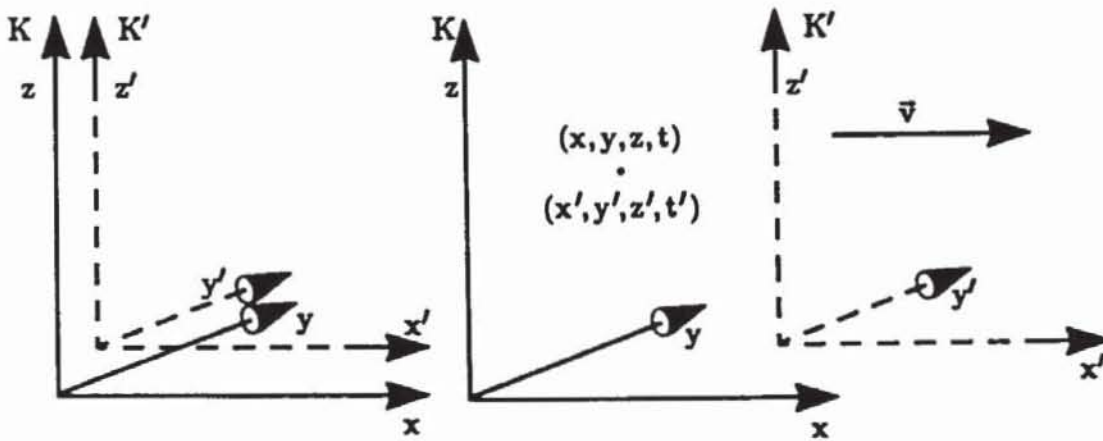


Fig. 2.6. Two coordinate systems K and K' moving relative to each other in X (and X') direction with the velocity V .

The main consequences are the Lorentz contraction of moving bodies, the time dilatation (better known as the famous twin paradoxon) and the strange properties of the relativistic theorem for adding velocities. For velocities in the range of human experience the relativistic effects are tiny. Even a racing car at a speed of 300 km/h is shortened by 1.5×10^{-13} m which is only 1/1000 of the diameter of an atom. But at velocities approaching the velocity of light $c = 300\,000$ km/s the effects become dramatic. However, it should be noted that the Lorentz transformation (2.15) tells us what we measure but not what we see.

2.4 Effects of signal propagation time

Especially in scientific visualisation, it might become necessary to distinguish between the kinematic behaviour which can already be quite complicated like in special relativity and the visual appearance of this behaviour for the observer. The only way we can experience the state of a distant object is by receiving physical signals from there. Those signals spread with a certain characteristic velocity which leads to the fact that a signal which was sent out from a part of the object which was further away is received at later time.

Therefore, a picture which we take of the object at a certain time contains information about the object at various time steps before. If, for example, one tries to animate what bats "see", one has to take into account the velocity of sound in air.

This effect is even more dramatic in special relativity where we have to deal with the finite velocity of light in order to gain a correct visual impression of the space-time structure. The picture we would see of a relativistic moving object is produced by photons which arrive at the same time at the eye or at a detector, but which were emitted from the object when it was at various positions. Fig. 2.7 shows that a straight rod, which is moving towards us at a very high speed will appear bent, because the photons from the outer parts have to travel a longer way than the ones from the inner parts and have thus to be started, when the rod was further away.

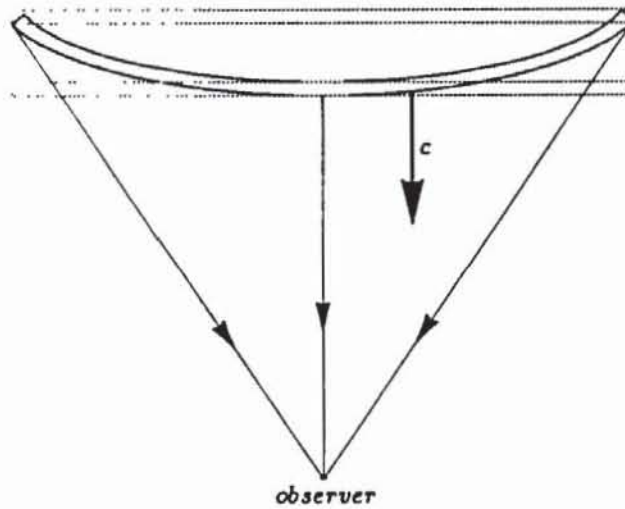


Fig. 2.7. A straight rod which is moving towards the observer with a velocity of almost the speed of light will appear bent, because the photons from the outer parts of the rod have to travel a longer way and therefore have to start earlier in order to arrive at the same time at the observer.

Combining the effects of the Lorentz-transformation (like contraction and aberration) and light travel time an even simple kinematic animation like flying with almost the velocity of light through Berlin's Brandenburg gate gives a visual impression one would naively have never expected (cf. Fig. 2.8) (Ertl et al., 1991).

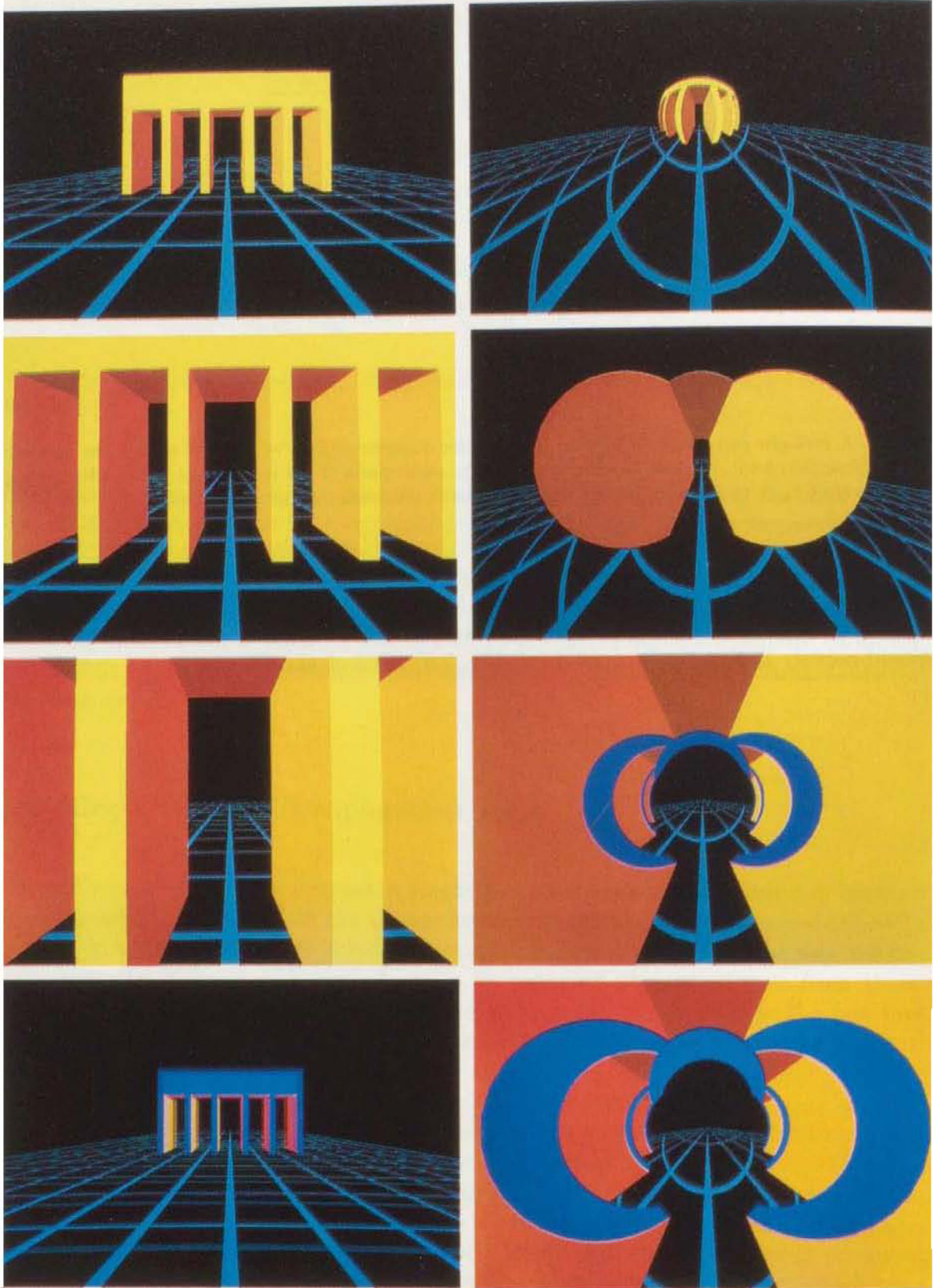


Fig. 2.8. A visualisation of the space-time structure of special relativity, when flying with various velocities through the Brandenburg gate. The four images on the left hand side show what the observer sees when he moves with 10% of the speed of light. The various sides of the building are colored differently for better orientation: the front is yellow, the rear is blue and the inner sides are red, brown and orange. In the bottom picture the observer has turned 180 degrees and looks back towards the rear side. The four images in the right column show what an observer would see, if he moved with 99% of the speed of light. The gate appears dramatically distorted and although the observer looks into the direction of the motion he is able to see the inner and the rear sides as well.

3 Basic principles of dynamics

In this chapter we will present a short review of the physical laws which are necessary to produce physically correct motion for computer animation. Dynamics describes the motion of point masses and rigid bodies under the influence of external forces.

3.1 Mechanics of point masses

In ordinary computer animation sequences the occurring velocities are much smaller than the velocity of light and the gravitational forces are small as well. Therefore, Newton's laws are the appropriate theory for correct description of the dynamical behaviour:

1. Without external forces, a body is at rest or moves with constant velocity on a straight line.
2. An external force \mathbf{F} acting on a body of mass m results in an acceleration \mathbf{a} with $\mathbf{F} = m\mathbf{a}$.
3. *actio = reactio* that means to every action corresponds a reaction in opposite direction and of equal size.

3.1.1 Newton's law for the motion of a point mass

The motion of a point mass m under the influence of an external force \mathbf{F} is given in an inertial frame by Newton's second law:

$$m\ddot{\mathbf{r}} = \mathbf{F} \quad (3.1)$$

Forces with constant magnitude corresponding to the kinematic examples in the last chapter are the gravity $\mathbf{F} = m\mathbf{g}$ and the centrifugal force $\mathbf{F} = m\omega^2\mathbf{r}$.

Eq. 3.1 is a differential equation of second order for the position vector \mathbf{r} . With given initial values at $t = 0$ for position \mathbf{r}_0 and velocity \mathbf{v}_0 and known force $\mathbf{F}(\mathbf{r}, t)$, the motion can immediately be calculated by integration of (3.1). This procedure is called *direct dynamics* and the result is the position vector $\mathbf{r} = \mathbf{r}(t)$ as a function of time.

$$\mathbf{a}(t) = \frac{1}{m}\mathbf{F}(t) \quad (3.2a)$$

$$\mathbf{v}(t) = \frac{1}{m} \int_0^t \mathbf{F}(t') dt' + \mathbf{v}_0 \quad (3.2b)$$

$$\mathbf{r}(t) = \frac{1}{m} \int_0^t \left(\int_0^{t'} \mathbf{F}(t'') dt'' \right) dt' + \mathbf{v}_0 t + \mathbf{r}_0 \quad (3.2c)$$

It is convenient to introduce the momentum \mathbf{p} :

$$\mathbf{p} = m\mathbf{v} \quad . \quad (3.3)$$

Newton's law then reads

$$\dot{\mathbf{p}} = \mathbf{F} \quad , \quad (3.4)$$

which leads to the consequence that without external forces momentum is conserved:

$$\mathbf{F} = 0 \quad \implies \mathbf{p} = \text{constant} \quad . \quad (3.5)$$

The angular momentum of a point mass with momentum \mathbf{p} with respect to the origin of the coordinate system is defined as

$$\mathbf{L} = \mathbf{r} \times \mathbf{p} \quad , \quad (3.6)$$

and the torque \mathbf{T} produced by a force acting at \mathbf{r} as

$$\mathbf{T} = \mathbf{r} \times \mathbf{F} \quad . \quad (3.7)$$

These quantities are used in the dynamic equation for rotation:

$$\dot{\mathbf{L}} = \frac{d}{dt}(\mathbf{r} \times \mathbf{p}) = \mathbf{r} \times \dot{\mathbf{p}} + \dot{\mathbf{r}} \times \mathbf{p} = \mathbf{r} \times \dot{\mathbf{p}} = \mathbf{T} \quad . \quad (3.8)$$

In the absence of external torques the angular momentum is conserved:

$$\mathbf{T} = 0 \quad \implies \mathbf{L} = \text{constant} \quad . \quad (3.9)$$

3.1.2 Relativistic dynamics of a point mass

For animation problems in our daily environment Newton's mechanics is the appropriate theory. For animation problems in astrophysics and above all in science fiction with velocities near the velocity of light, the special theory of relativity must be applied. Besides the different kinematics discussed in Sect. 2.3, there are also modifications in dynamics compared with Newton's theory.

For a point mass the relativistic equations of motion are formally quite similar to Newton's equations

$$\frac{d\mathbf{p}}{dt} = \mathbf{F} \quad (3.10a)$$

$$\frac{dE}{dt} = \mathbf{F} \cdot \mathbf{v} \quad . \quad (3.10b)$$

The essential difference is that the relativistic momentum \mathbf{p} and the relativistic energy E for a mass point with rest mass m_0 has the form

$$\mathbf{p} = \frac{m_0\mathbf{v}}{\sqrt{1 - (\frac{v}{c})^2}} \quad (3.11a)$$

$$E = \frac{m_0c^2}{\sqrt{1 - (\frac{v}{c})^2}} \quad (3.11b)$$

with the consequence that for any object the velocity of light c is the limiting velocity.

The treatment of extended bodies in the frame of a relativistic theory is a highly complicated task and far beyond the scope of this tutorial. Even the terminus rigid body is not allowed, since in a rigid body the sound velocity is infinite and therefore larger than c .

3.1.3 Non-inertial coordinate systems

For some purposes it can be convenient to observe the motion from a moving, an accelerated or a rotating system. There are two ways to solve this problem. The first is to solve (3.1) in the inertial system and then to transform the solution into the desired system. The other possibility, which is completely equivalent to the first, is to transform (3.1) into the non-inertial system. When transforming into a rotating system we use the general law for the transformation of the time derivative

$$\frac{d}{dt} = \frac{d'}{dt} + \boldsymbol{\omega} \times, \quad (3.12)$$

where $\frac{d'}{dt}$ denotes the time derivative in the rotating system. The resulting modified equation of motion contains additional terms. E.g., in the transition to a rotating system with the angular velocity $\boldsymbol{\Omega}(t)$ terms describing Coriolis forces, centrifugal forces and forces caused by the time dependence of $\boldsymbol{\Omega}$ arise:

$$m \frac{d^2 \mathbf{r}}{dt^2} = \mathbf{F} - 2m\boldsymbol{\Omega} \times \frac{d' \mathbf{r}}{dt} - m\boldsymbol{\Omega} \times (\boldsymbol{\Omega} \times \mathbf{r}) - m\dot{\boldsymbol{\Omega}} \times \mathbf{r} . \quad (3.13)$$

Although (3.13) seems to be far more complicated there are many cases, where (3.13) is the better formulation. One example is the motion of particles in a binary system with two orbiting stars as presented in Fig. 3.1.

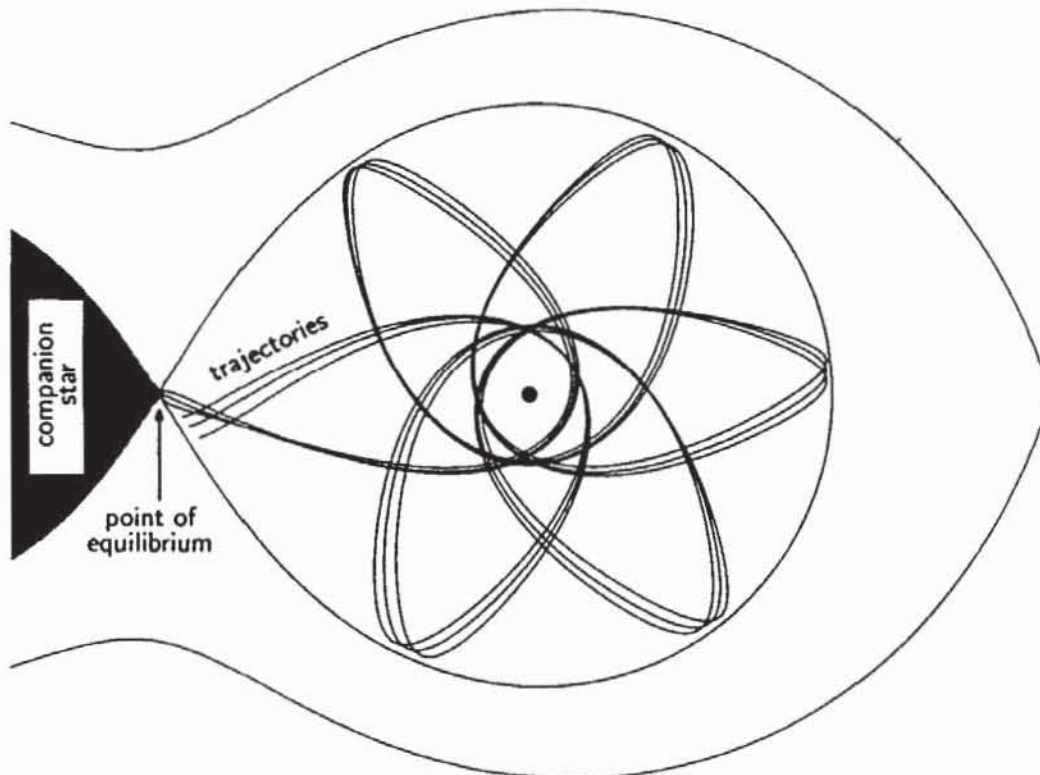


Fig. 3.1. The trajectories of particles in a rotating frame under influence of the gravitational forces of two orbiting stars

3.1.4 Computer animation by particle simulation

The method of particle simulation is a powerful tool to treat hydrodynamic problems. Furthermore, this approach automatically leads to animation sequences. The basic idea is to replace the $10^{25} - 10^{60}$ atoms or molecules of a macroscopic gaseous or fluid object by $10^4 - 10^5$ pseudo particles which interact in such a way that the macroscopic properties like pressure or viscosity are correctly simulated. The equations of motion of these pseudo particles including all external and internal forces are integrated and macroscopic physical quantities are derived from the positions and velocities of the particles. In order to obtain smooth simulation pictures the pseudo particles are smeared out to a continuous density.

A good example for this very general method is the formation of an accretion disk in a close binary system (Ruder et al., 1990). Such a system consists of a normal star and a degenerated object, e.g. a white dwarf star, a neutron star or a black hole. The normal star fills its Roche volume and matter flows from the equilibrium point between the two stars to the compact object and forms a disk caused by the angular momentum of the overflowing matter. In the corotating system of the two stars the dynamic equation which must be solved for each particle has the form

$$\frac{d^2 \mathbf{v}}{dt^2} = \nabla \left(\frac{Gm_1}{|\mathbf{r}_1 - \mathbf{r}|} + \frac{Gm_2}{|\mathbf{r}_2 - \mathbf{r}|} \right) - 2\boldsymbol{\Omega} \times \mathbf{v} - \boldsymbol{\Omega} \times (\boldsymbol{\Omega} \times \mathbf{r}) - \frac{1}{\rho} \nabla P + \nu \Delta \mathbf{v}, \quad (3.14)$$

where, on the right hand side, the terms represent the gravitational forces of the two stars, the Coriolis force, the centrifugal force, the pressure (ρ is the density) and the viscosity.

Due to viscous interaction the orbits around the compact object become circular, mass flows inwards and angular momentum flows outwards in the disk. In Fig. 3.2 some snapshots of the time evolution series are shown. In addition, the viscosity causes dissipation of energy, which leads to a local temperature. A realistic animation sequence is obtained by converting the corresponding spectral (Planck) distribution for these temperatures to colours on a graphic screen. For the simulation of a stationary disk, as shown in Fig. 3.3, 40 000 pseudo particles are necessary and the computation based on a well vectorized code requires more than a day of cpu time on a Cray 2 supercomputer.

3.2 Euler's equations for the motion of a rigid body

A point mass is a very special case for animation purposes. More general, the objects, which should be animated, are rigid bodies or systems of rigid bodies connected by joints. A rigid body is defined by its total mass M and its tensor of inertia $\underline{\underline{\Theta}}$, which in a body-fixed $\xi\eta\zeta$ -system with the origin in the center of mass has the following form

$$\underline{\underline{\Theta}} = \begin{pmatrix} \int (\eta^2 + \zeta^2) \rho d\tau' & - \int \xi \eta \rho d\tau' & - \int \xi \zeta \rho d\tau' \\ - \int \xi \eta \rho d\tau' & \int (\xi^2 + \zeta^2) \rho d\tau' & - \int \eta \zeta \rho d\tau' \\ - \int \xi \zeta \rho d\tau' & - \int \eta \zeta \rho d\tau' & \int (\xi^2 + \eta^2) \rho d\tau' \end{pmatrix}. \quad (3.15)$$

$\rho = \rho(\xi, \eta, \zeta)$ is the local density of matter and $d\tau' = d\xi d\eta d\zeta$ is the volume element.

Its position and orientation in space is defined by the three cartesian coordinates x_c, y_c, z_c for the position of the center of mass and by the three Euler angles α, β, γ for

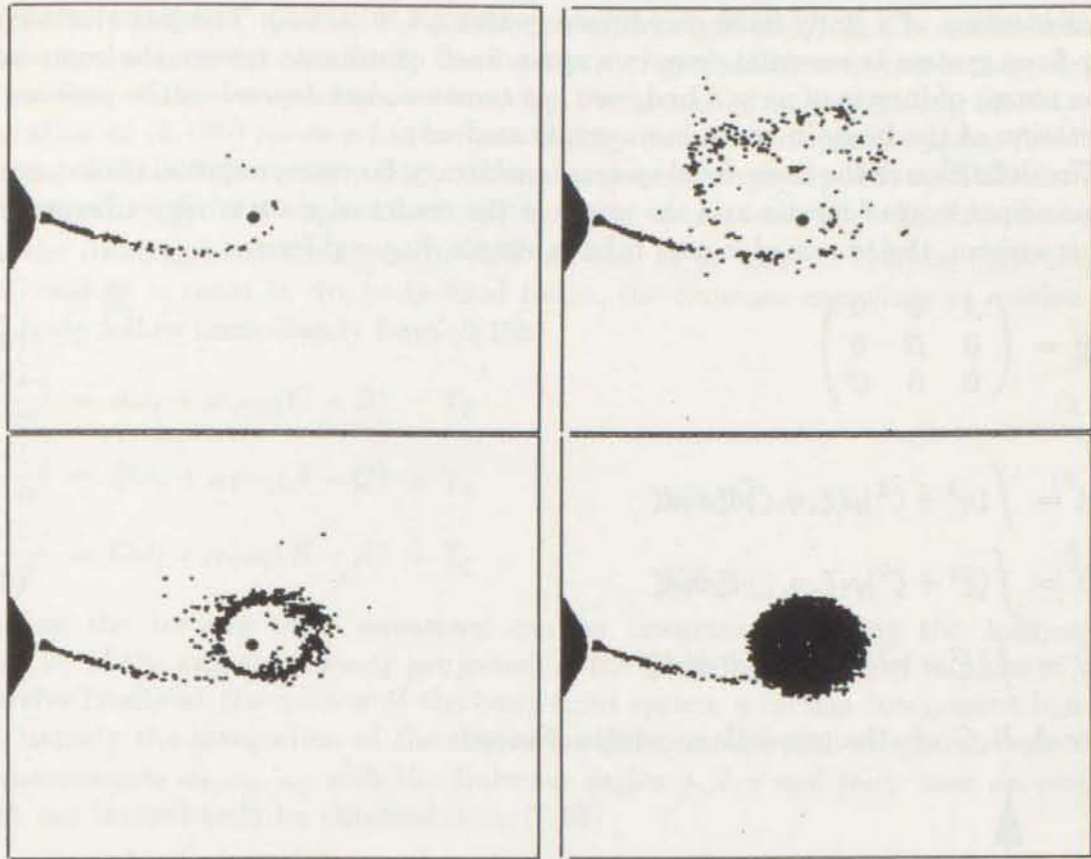


Fig. 3.2. A time series showing the formation of an accretion disk as a result of a dynamic computer simulation. Because of the gravitational pull of the compact object, matter is pulled away from the red star forming a thin disk around the white dwarf.

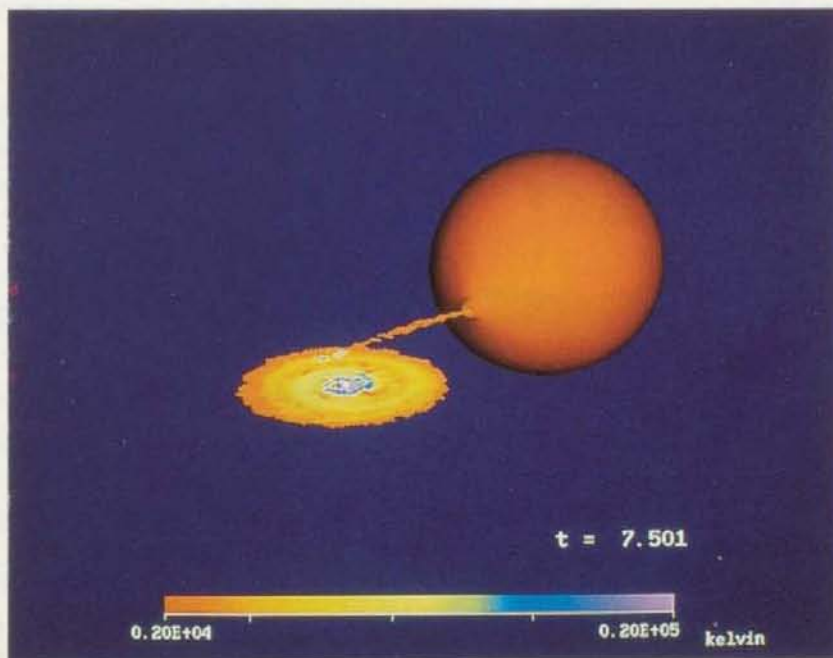


Fig. 3.3. An evolved stationary accretion disk where the color coding represents the local temperature produced by viscous interaction of the particles.

the orientation of a body-fixed coordinate system (cf. Fig. 2.5). The introduction of a body-fixed system is essential since in a space-fixed coordinate system the components of the tensor of inertia of a rigid body are not constant, but depend on the position and orientation of the body in space in a complicated way.

The definition of the body-fixed system is arbitrary, however, a special choice, namely the principal axes of inertia and the origin in the center of mass is very advantageous. In this system, the tensor of inertia takes a simple diagonal form

$$\underline{\underline{\Theta}} = \begin{pmatrix} A & 0 & 0 \\ 0 & B & 0 \\ 0 & 0 & C \end{pmatrix} \quad (3.16)$$

with

$$\begin{aligned} A &= \int (\eta^2 + \zeta^2) \rho(\xi, \eta, \zeta) d\xi d\eta d\zeta \\ B &= \int (\xi^2 + \zeta^2) \rho(\xi, \eta, \zeta) d\xi d\eta d\zeta \\ C &= \int (\xi^2 + \eta^2) \rho(\xi, \eta, \zeta) d\xi d\eta d\zeta \quad , \end{aligned} \quad (3.17)$$

where A, B, C are the principle moments of inertia.

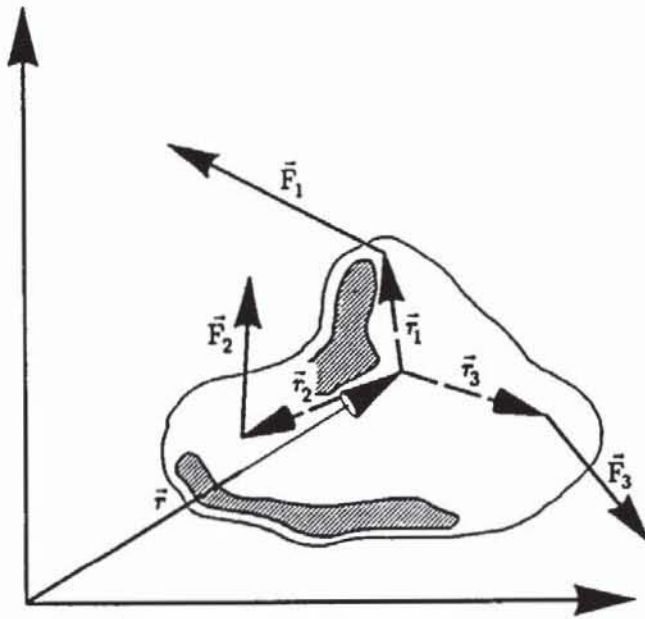


Fig. 3.4. Forces acting on a rigid body

In general, a number of forces act on the rigid body (cf. Fig. 3.4) and the problem is the resulting motion in space. Using center-of-mass coordinates x_c, y_c, z_c and fixing the origin of the body-fixed $\xi\eta\zeta$ -system at the center of mass the equations of motion for the system decouple in an equation for the center of mass and one relative to it:

$$M\vec{R}_c = \dot{\vec{P}} = \sum_i \vec{F}_i \quad , \quad (3.18a)$$

$$\dot{\vec{L}} = \frac{d}{dt}(\underline{\underline{\Theta}}\omega) = \sum_i (\vec{r}'_i \times \vec{F}_i) + \sum_i \vec{T}_i \quad . \quad (3.18b)$$

Here $M = \int \rho d\xi d\eta d\zeta$ denotes the total mass of the rigid body, F_i the external forces, L the angular momentum and T_i the external torques relative to the center of mass. The motion of the center of mass can easily be calculated by integrating (3.18a). The integration of (3.18b) needs a further processing since with respect to space-fixed axes the components of the tensor of inertia are, in general, time-dependent. Therefore, the time derivative $\frac{d}{dt}$ in the space-fixed system must be expressed by the time derivative $\frac{d'}{dt}$ in the rotating body-fixed system with the help of the general relation (3.12). Using (3.12) and $\underline{\Theta} = \text{const}$ in the body-fixed frame, the Eulerian equations of motion of a rigid body follow immediately from (3.18b)

$$\frac{dL_\xi}{dt} = A\dot{\omega}_\xi + \omega_\eta\omega_\zeta(C - B) = T_\xi \quad (3.19a)$$

$$\frac{dL_\eta}{dt} = B\dot{\omega}_\eta + \omega_\xi\omega_\zeta(A - C) = T_\eta \quad (3.19b)$$

$$\frac{dL_\zeta}{dt} = C\dot{\omega}_\zeta + \omega_\xi\omega_\eta(B - A) = T_\zeta \quad (3.19c)$$

Knowing the torques these equations can be integrated, yielding the components $\omega_\xi, \omega_\eta, \omega_\zeta$ of the angular velocity projected on the body-fixed axes as functions of time. To arrive finally at the motion of the body-fixed system a further integration is necessary, namely the integration of the first-order differential equation system connecting the components $\omega_\xi, \omega_\eta, \omega_\zeta$ with the Eulerian angles α, β, γ and their time derivatives, which can immediately be obtained from (2.13)

$$\dot{\alpha} = -\frac{1}{\sin\beta}(\omega_\xi \cos\gamma + \omega_\eta \sin\gamma) \quad (3.20a)$$

$$\dot{\beta} = \omega_\xi \sin\gamma + \omega_\eta \cos\gamma \quad (3.20b)$$

$$\dot{\gamma} = \omega_\xi \cot\beta \cos\gamma - \omega_\eta \cot\beta \sin\gamma + \omega_\zeta \quad (3.20c)$$

Eqs. (3.1), (3.18a) and (3.20) represent the basic equations of motion for a point mass and for a rigid body. With given initial conditions for position and velocity and known external forces and torques the position of the center of mass and the orientation of the body-fixed axes can be calculated by means of a standard integration routine.

3.3 A simple example: the falling rod

To warm up let us consider as a simple example a rod freely falling down from a certain height, hitting the bottom and jumping off again. The rod possesses the mass M and the length l . Its tensor of inertia $\underline{\Theta}$ relative to the center of mass and in the body-fixed system of the principle axes of inertia is of the form

$$\underline{\Theta} = \begin{pmatrix} A & 0 & 0 \\ 0 & A & 0 \\ 0 & 0 & 0 \end{pmatrix} \quad (3.21)$$

with $A = \frac{1}{12}Ml^2$.

The rod is described by the three Cartesian coordinates x_c, y_c, z_c of its center of mass lying in the middle of the rod and by the two Eulerian angles α, β for the orientation. The third Eulerian angle γ is without meaning since the principle moment of inertia around the axis is zero and, therefore, the rod is not able to rotate around this axis

with the consequence that ω_z is zero. In free fall, the only external force is the gravity Mg which acts on the center of mass. This is also the reason why the external torques vanish.

Taking into account the above considerations the equations of motion (3.18a) and (3.19) simplify to

$$M\ddot{x}_c = 0 \quad (3.22a)$$

$$M\ddot{y}_c = 0 \quad (3.22b)$$

$$M\ddot{z}_c = -Mg \quad (3.22c)$$

$$\dot{\omega}_\xi = 0 \quad (3.22d)$$

$$\dot{\omega}_\eta = 0 \quad , \quad (3.22e)$$

which immediately can be solved analytically, yielding

$$x_c = v_{cx0}t + x_{c0} \quad (3.23a)$$

$$y_c = v_{cy0}t + y_{c0} \quad (3.23b)$$

$$z_c = -\frac{1}{2}gt^2 + v_{cz0}t + z_{c0} \quad (3.23c)$$

$$\omega_\xi = \omega_{\xi 0} \quad (3.23d)$$

$$\omega_\eta = \omega_{\eta 0} \quad , \quad (3.23e)$$

where the values of the position and velocity of the initial state are denoted by an index zero.

The motion of the rod is the superposition of the parabola of its center of mass and a rotation with constant angular velocity $\omega = \sqrt{\omega_\xi^2 + \omega_\eta^2}$ around an axis perpendicular to the rod. The explicit time dependence of the Eulerian angles can be obtained by integrating (3.20)

$$\tan \alpha = \tan(\omega t) / \sin \beta_{\min} \quad (3.24a)$$

$$\cos \beta = \cos(\omega t) \cos \beta_{\min} \quad , \quad (3.24b)$$

where β_{\min} is the smallest angle between the axis of the rod and the z -axis, which occurs during the rotation.

The falling and rotating rod is also an appropriate example to discuss basically what happens during an impact. To demonstrate more clearly the essential idea we simplify the motion and assume that the rod rotates in the same plane in which its center of mass moves. This means $\alpha = 0$. To be consistent with later notation we introduce the angle $\varphi = 90^\circ - \beta$ for the orientation of the rod. Fig. 3.5 shows the situation at the moment of impact.

The motion is completely described by

$$x_c = v_{cx0}t + x_{c0} \quad (3.25a)$$

$$z_c = -\frac{1}{2}gt^2 + v_{cz0}t + z_{c0} \quad (3.25b)$$

$$\varphi = -\omega_y t + \varphi_0 \quad . \quad (3.25c)$$

With x_e, z_e we denote the Cartesian coordinates of the lower impacting end of the rod, which are geometrically related to the coordinates x_c, z_c, φ by

$$x_e = x_c - \frac{l}{2} \cos \varphi \quad (3.26a)$$

$$z_e = z_c - \frac{l}{2} \sin \varphi \quad . \quad (3.26b)$$

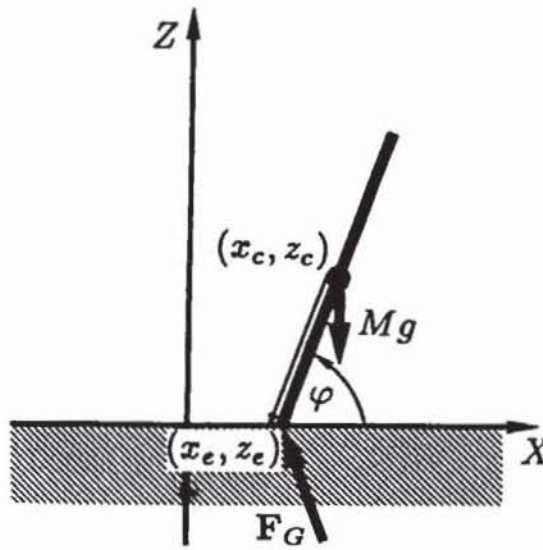


Fig. 3.5. Coordinates and external forces of a rigid rod during impact

The time derivative of (3.26) yields for the corresponding velocities

$$\dot{x}_e = \dot{x}_c + \frac{l}{2} \sin \varphi \dot{\varphi} \quad (3.27a)$$

$$\dot{z}_e = \dot{z}_c - \frac{l}{2} \cos \varphi \dot{\varphi} \quad (3.27b)$$

As a further notation we introduce the upper indices *impact* for the values of the quantities at the time of the impact, *before* for immediately before and *after* for immediately after the impact.

Assuming the rod and the bottom to be infinitely rigid the duration of the impact is infinitely short and the ground reaction force F_G is a δ -peak. The integration of the equations of motion

$$M\ddot{x}_c = F_{Gx}(t) = c_x \delta(t^{\text{impact}}) \quad (3.28a)$$

$$M\ddot{z}_c = -Mg + F_{Gz}(t) = -Mg + c_z \delta(t^{\text{impact}}) \quad (3.28b)$$

$$\Theta \ddot{\varphi} = (x_e^{\text{impact}} - x_c) F_{Gz} - (z_e^{\text{impact}} - z_c) F_{Gx} \quad (3.28c)$$

over the infinitesimally short impact time leads to the relations between the changes of the linear and angular momenta and the integral of the impact forces and torques

$$M(\dot{x}_c^{\text{after}} - \dot{x}_c^{\text{before}}) = M\Delta\dot{x}_c = \int_{t^{\text{impact}}-\epsilon}^{t^{\text{impact}}+\epsilon} F_{Gx}(t') dt' = c_x \quad (3.29a)$$

$$M(\dot{z}_c^{\text{after}} - \dot{z}_c^{\text{before}}) = M\Delta\dot{z}_c = \int_{t^{\text{impact}}-\epsilon}^{t^{\text{impact}}+\epsilon} [-Mg + F_{Gz}(t')] dt' = c_z \quad (3.29b)$$

$$\Theta(\dot{\varphi}^{\text{after}} - \dot{\varphi}^{\text{before}}) = \Theta\Delta\dot{\varphi} = (x_e^{\text{impact}} - x_c)c_z - (z_e^{\text{impact}} - z_c)c_x \quad (3.29c)$$

To calculate explicitly these changes further information on the mechanical properties of the ground is necessary. Two limiting cases are on the one hand a totally elastic behaviour and on the other hand a totally inelastic behaviour. In the first case the z -component of the velocity of the impacting end \dot{z}_e of the rod alters its sign and the second equation for determining the constants c_x and c_z is the conservation of the

total energy during the impact. In the second case the end of the rod comes to rest immediately after the impact, which yields the two additional equations desired.

Let us first look to the totally elastic case. The equation of the reversal of the z -velocity reads

$$\dot{z}_e^{\text{after}} = -\dot{z}_e^{\text{before}} \implies \quad (3.30a)$$

$$\begin{aligned} \Delta \dot{z}_e &= \dot{z}_e^{\text{after}} - \dot{z}_e^{\text{before}} \\ &= \dot{z}_c^{\text{after}} - \frac{l}{2} \cos(\varphi^{\text{impact}}) \dot{\varphi}^{\text{after}} - \dot{z}_c^{\text{before}} + \frac{l}{2} \cos(\varphi^{\text{impact}}) \dot{\varphi}^{\text{before}} \\ \implies \Delta \dot{z}_c - \frac{l}{2} \cos(\varphi^{\text{impact}}) \Delta \dot{\varphi} &= -2\dot{z}_e^{\text{before}} \quad , \end{aligned} \quad (3.30b)$$

and the conservation of the total energy during the impact leads to

$$\begin{aligned} E^{\text{after}} - E^{\text{before}} &= 0 \implies \\ \frac{1}{2} M [(\dot{x}_c^{\text{after}})^2 + (\dot{z}_c^{\text{after}})^2] + M g z_c^{\text{impact}} + \frac{1}{2} \Theta (\dot{\varphi}^{\text{after}})^2 \\ - \frac{1}{2} M [(\dot{x}_c^{\text{before}})^2 + (\dot{z}_c^{\text{before}})^2] - M g z_c^{\text{impact}} - \frac{1}{2} \Theta (\dot{\varphi}^{\text{before}})^2 \\ &= \frac{1}{2} M [\Delta \dot{x}_c (\Delta \dot{x}_c + 2\dot{x}_c^{\text{before}}) + \Delta \dot{z}_c (\Delta \dot{z}_c + 2\dot{z}_c^{\text{before}})] \\ &\quad + \frac{1}{2} \Theta [\Delta \dot{\varphi} (\Delta \dot{\varphi} + 2\dot{\varphi}^{\text{before}})] = 0 \quad . \end{aligned} \quad (3.30c)$$

Eqs. (3.30b,c) and (3.29c) determine the changes of the velocities during the impact. The values of the quantities immediately before the impact can be calculated from the solution (3.25) and depend uniquely on the initial conditions. Having the changes at hand the values of the positions at the impact and the values of the velocities immediately after the impact serve as initial conditions for the further motion until the next impact.

In the second case of a totally inelastic impact with $\dot{x}_e^{\text{after}} = 0$ and $\dot{z}_e^{\text{after}} = 0$ the equations read

$$\begin{aligned} \Delta \dot{x}_e &= \dot{x}_e^{\text{after}} - \dot{x}_e^{\text{before}} = -\dot{x}_e^{\text{before}} \implies \\ \Delta \dot{x}_c &= \dot{x}_c^{\text{after}} + \frac{l}{2} \sin(\varphi^{\text{impact}}) \dot{\varphi}^{\text{after}} - \dot{x}_c^{\text{before}} - \frac{l}{2} \sin(\varphi^{\text{impact}}) \dot{\varphi}^{\text{before}} \\ \implies \Delta \dot{x}_c + \frac{l}{2} \sin(\varphi^{\text{impact}}) \Delta \dot{\varphi} &= -\dot{x}_e^{\text{before}} \quad , \end{aligned} \quad (3.31a)$$

$$\begin{aligned} \Delta \dot{z}_e &= \dot{z}_e^{\text{after}} - \dot{z}_e^{\text{before}} = -\dot{z}_e^{\text{before}} \implies \\ \Delta \dot{z}_c &= \dot{z}_c^{\text{after}} - \frac{l}{2} \cos(\varphi^{\text{impact}}) \dot{\varphi}^{\text{after}} - \dot{z}_c^{\text{before}} + \frac{l}{2} \cos(\varphi^{\text{impact}}) \dot{\varphi}^{\text{before}} \\ \implies \Delta \dot{z}_c - \frac{l}{2} \cos(\varphi^{\text{impact}}) \Delta \dot{\varphi} &= -\dot{z}_e^{\text{before}} \quad , \end{aligned} \quad (3.31b)$$

From (3.31a,b) and (3.29c) with the same procedure as above the motion can further be monitored. Of course, in this case the total energy is not conserved. In Fig. 3.6 three stroboscopic time series of a falling rod are shown for different elastic behaviour of the ground.

In the above considerations the impact is a point event in time. If one is interested in details during the impact the mechanical properties of the colliding parts must be taken into account. This requires the knowledge of the relation between the reaction

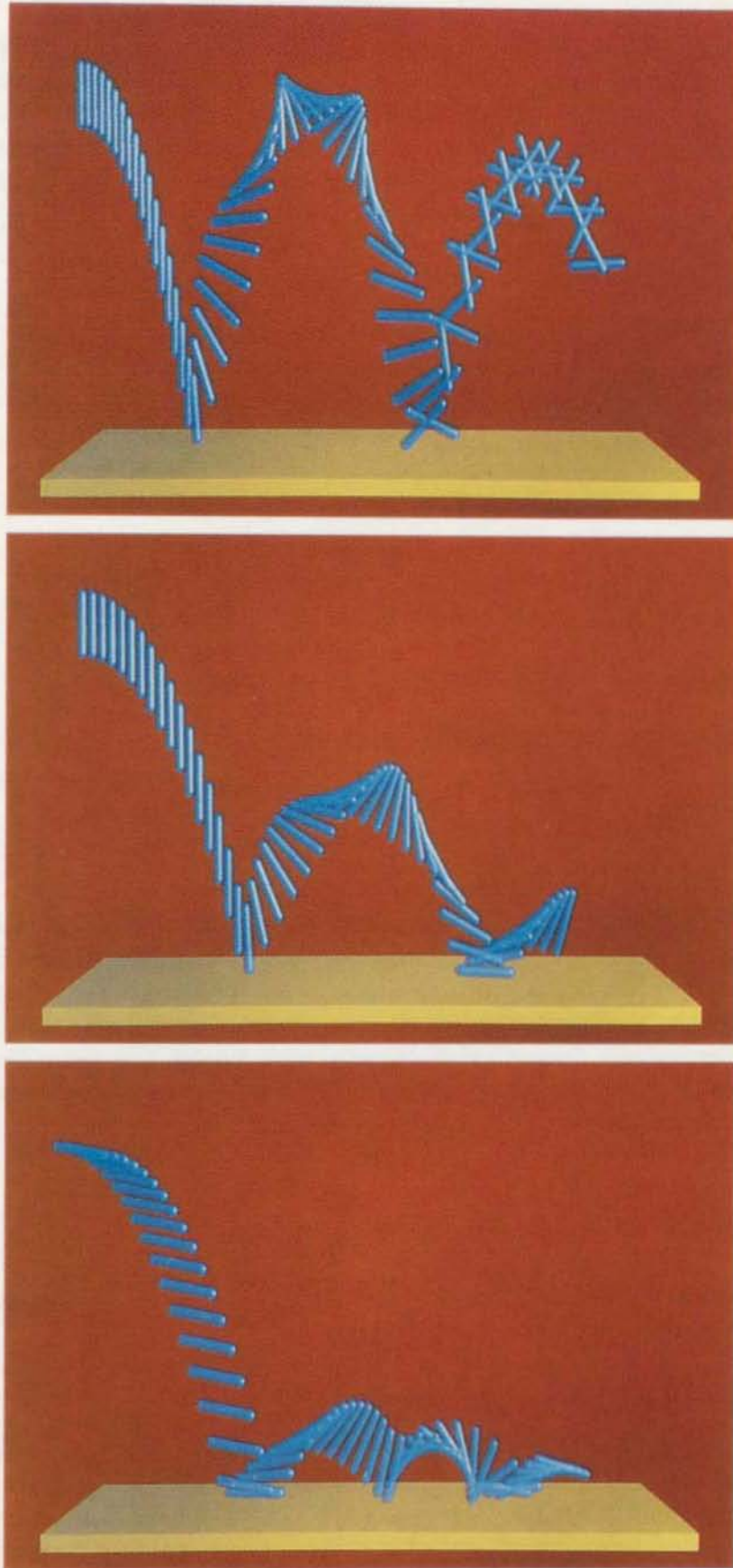


Fig. 3.6. Three stroboscopic time series of a falling rod for an increasing (top to bottom) damping component in the ground reaction force.

force and the local deformation and, if damping elements are present, the instantaneous deformation velocity. Inserting a realistic relation $F_G(r_{\text{deform}}, \dot{r}_{\text{deform}})$ into the right hand sides of (3.28) and integrating numerically these equations yield all quantities as continuous functions of time even in the impact region, which is now extended in a small time interval. As an example for a specific ground behaviour the following relations could be used as components of the ground reaction force:

$$F_{Gz} = a (z_{\text{deform}})^b + d \dot{z}_{\text{deform}} \quad ; \quad F_{Gx} = \mu F_{Gz} \quad . \quad (3.32)$$

The vertical component of the ground reaction force depends on the deformation and on the deformation velocity of the ground; a , b and d are material constants. The horizontal component of the ground reaction force is usually determined by friction and therefore proportional to F_{Gz} .

4 Mechanics of multi-linked models for biomechanical simulations

For the modelling of human beings or animals with legs and arms multi-linked systems of extended bodies connected by joints are necessary. Developing a satisfactory model is by no means a trivial problem. The joints and their constraints must be correctly described as well as the mechanical properties of the body segments. Important is the action of external forces especially during short impacts and, finally, the time development of the internal torques in the joints, which are generated by the skeletal muscles and thus reflect the free will of the being to control its motion.

4.1 Description of a multi-linked system

In principle, the mechanical problem of a multi-linked system has been solved for a long time. We will recapitulate some general facts.

4.1.1 Coordinates and degrees of freedom

Let us consider a system with n segments and $n - 1$ joints. At first, we will assume that the motion takes place in a plane. Then, each segment is defined by three coordinates, two cartesian coordinates for the position of the center of mass and one angle for the orientation (cf. Fig. 4.1a).

All together we have $3n$ coordinates and, therefore, we need $3n$ equations. In the plane case each joint yields two conditions, namely that the coordinates of the two end points of corresponding segments coincide. Taking into account these conditions we end up with $3n - 2(n - 1) = n + 2$ degrees of freedom. The number $n + 2$ is also the minimal number of coordinates needed for a unique description. These coordinates are free from

any restrictions. Additionally, we have three equations of motion, two for the center of mass of the whole system and one for the motion relative to it. Thus, there remain $n + 2 - 3 = n - 1$ quantities undetermined, the torques in the $n - 1$ joints, the free will of the individual.

An other way to consider the same subject is to regard each segment separately. In our plane case we need 3 coordinates $(x_{ci}, z_{ci}, \varphi_i)$ for each segment and, with known forces and torques acting on the segment, the motion of its center of mass and relative to it can be obtained by numerically integrating the 3 equations of motion

$$M_i \ddot{x}_{ci} = \sum_j F_{ijx} \quad (4.1a)$$

$$M_i \ddot{z}_{ci} = \sum_j F_{ijz} \quad (4.1b)$$

$$\Theta_i \ddot{\varphi}_i = \sum_j (x_{ij} F_{ijz} - z_{ij} F_{ijx}) - \sum_j T_{ijy} \quad (4.1c)$$

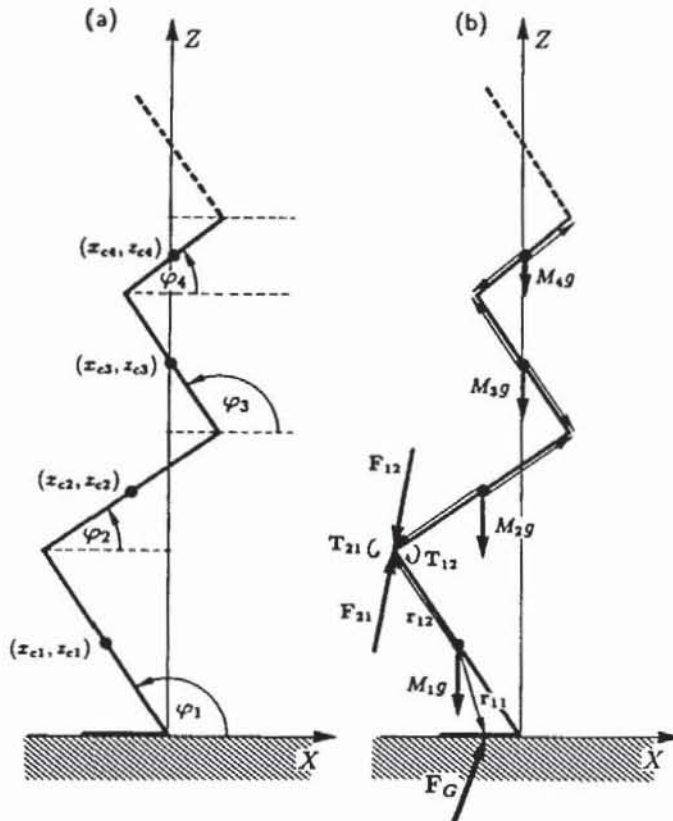


Fig. 4.1. (a) Coordinates of a plane multi-linked system. Each segment is defined by the Cartesian coordinates x_{ci}, z_{ci} of its center of mass and an angle φ_i determining its orientation relative to the horizontal line. (b) Forces and torques acting on the segments. Beside the external forces like gravitation and ground reaction force additionally, for the first joint, the internal forces and torques are shown.

$\sum_j F_{ij}$ and $\sum_j T_{ij}$ contain all forces and torques, external and internal, acting on the segment. The external forces such as gravitation, friction or contact forces must be given, the internal forces are caused by the constraints of the joints. Due to *actio = reactio* there are two unknown force components at a joint acting in opposite direction on the two segments connected by this joint. Since the condition of a joint yields two equations, the $2(n - 1)$ internal forces are uniquely determined by the $2(n - 1)$ equations

of the joint conditions. These forces are necessary to keep the segments together. The standard method to deal with such problems is the Lagrangian formalism. Solving the $3n + 2(n - 1)$ equations, the motion of the n connected segments and the internal joint forces are obtained simultaneously. The $(n - 1)$ torques, of course, are free again and determine the active behaviour of the model.

The same counting rhymes can be applied to a three dimensional model. To determine the degrees of freedom we note that one segment needs six coordinates and the $n - 1$ joints yield $3(n - 1)$ conditions thus, the minimal number of free coordinates is given by $6n - 3(n - 1) = 3n + 3$. Taking into account the six equations of motion for the whole system, we end up with $3(n - 1)$ freely choosable internal torques. This number, however, is only valid for freely movable spherical ball joints.

4.1.2 Joints and constraints

In the simulation of the motion of animals or human beings the modelling of joints is an essential part. Simple cases are hinge joints, which are movable around definite axes, or spherical ball joints, which are freely movable in three dimensions. For such joints the conditions for the connection of the two segments can easily be formulated as algebraic equations. An example for a ball joint is the human hip, one for a hinge joint is the human knee. The last is true only in a first approximation, a closer inspection exhibits a complex structure shown in Fig 4.2.



Fig. 4.2. Skeletal structure of the human knee joint with the different muscle and joint forces.

Far more complicated are joints without axes or points of rotation. Biological examples of such joints are the shoulders. Joints of this type can be modelled by introducing appropriate trunk-fixed and arm-fixed surfaces, which roll and slide on each other. These surfaces must be individually determined with the help of film analysis.

A further important aspect in modelling joints is the range of mobility. Each joint possesses a definite range of angles for flexion depending on the structure of the skeleton. During the course of animation sequences care must be taken that the joint angles do not exceed these biological limits. Of course, the most promising way is to imitate nature. When approaching the limiting angle in the joint an internal torque is built up which decelerates the motion and prevents an overshooting. This torque must depend on the difference of the actual joint angle and the limiting angle φ_{limit} and on the angular velocity of the joint angle. This velocity dependence is necessary to include a damping mechanism and thus to avoid an unnatural elastic reflection from the stop. A reasonable form of this torque is

$$T(|\varphi_{\text{limit}} - \varphi_{\text{joint}}|, \dot{\varphi}_{\text{joint}}) = \begin{cases} [a(|\varphi_{\text{limit}} - \varphi_{\text{joint}}|)^b + c]^{-1}(1 + d\dot{\varphi}_i) & \text{for } |\varphi_{\text{limit}} - \varphi_{\text{joint}}| \leq \varphi_{\text{on}} \\ 0 & \text{for } |\varphi_{\text{limit}} - \varphi_{\text{joint}}| > \varphi_{\text{on}} \end{cases}, \quad (4.2)$$

where a, b, c, d and φ_{on} are adjustable parameters. For a certain joint the angle φ_{on} denotes how many degrees before φ_{limit} the limiting torque starts to act. Typical values for φ_{on} are of the order of a few degrees.

4.2 The wobbling mass

In trying to simulate motion with high accelerations with a multi-linked system consisting of rigid bodies as segments the limits of such a model soon become obvious. The reasons for this failure are easily recognized by considering a high-speed movie of a jump or of an impact. The segments of the human body, trunk, thigh, lower leg, arms are far away from reacting like rigid bodies during an impact. Therefore, it is necessary to take into account the different composition of the body, namely the rigid skeletal part and the soft components like tendons, muscles, organs, and last but not least fat.

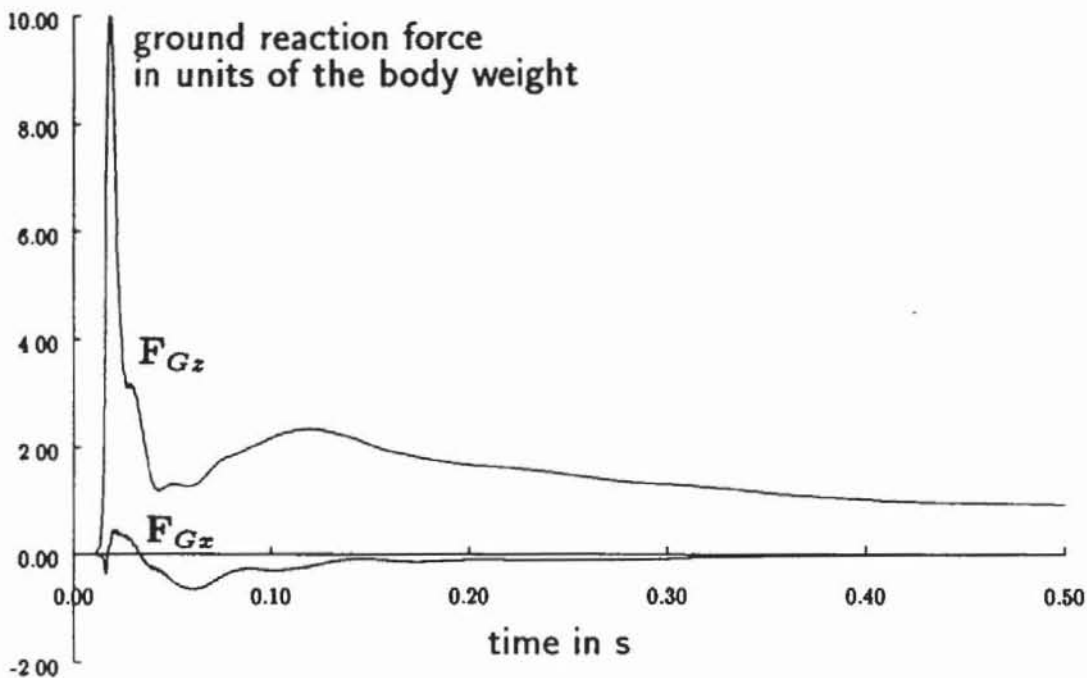


Fig. 4.3. Measured ground reaction force as a function of time for a down jump with landing on the heel.

For a better understanding of this requirement we roughly estimate what happens during the impact after a down jump of a human body from a height of 1 meter. The landing velocity is about 4.4 m/s. The heel is stopped within about 1 cm. Assuming for simplicity a constant deceleration this stopping length leads to a deceleration of 100 times the acceleration of gravity and it acts for about 5 milliseconds. During this time the skeletal part of the lower leg comes to rest. The wobbling mass of the body, however, remains almost in free fall, covers 3 to 4 cm and is then smoothly decelerated by the forces coupling it to the skeleton which is already at rest. The measurement of

the time evolution of a typical ground reaction force, shown in Fig. 4.3, clearly exhibits this behaviour. The height of the impact peak is about eight times the body weight and not 100 times and the width is about 20 ms and not 5 ms. A model consisting only of rigid bodies yields totally wrong results, especially, if the internal forces, which are of special interest in biomechanical research, are calculated. The further course of the ground reaction forces, the active phase, is determined by intentionally produced torques in the joints. In this region of the motion with smaller accelerations the wobbling mass is of secondary importance.

A correct modelling of the human body, e.g. with finite element methods, is extremely expensive and an animation based on this level nearly hopeless. A simple, practicable and very successful method to model the essential properties is to introduce a *wobbling mass* (Gruber et al., 1987, 1991), which summarizes all the soft parts of a segment and which is coupled quasi-elastically and strongly damped to the skeletal part. This wobbling mass can be moved and rotated relative to the skeleton as shown in Fig. 4.4.

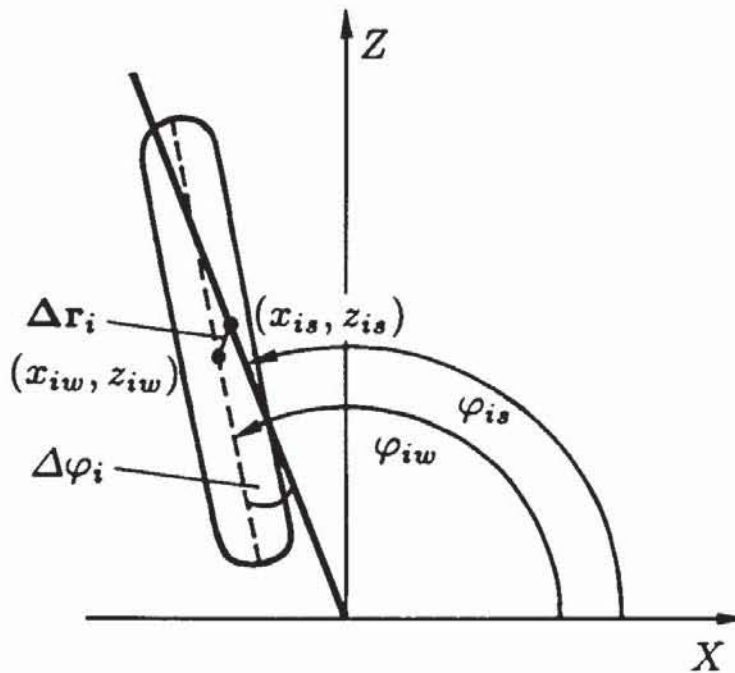


Fig. 4.4. Plane model of one body segment consisting of a skeletal part and a coupled wobbling mass, which is movable relative to the skeletal part. The displacement of the centers of mass is described by Δr_i , and the relative rotation by $\Delta \varphi_i$.

The additional coordinates needed to describe the wobbling mass are for each segment in the plane case two Cartesian coordinates $\Delta x_i, \Delta z_i$, for the displacement of the center of mass of the wobbling mass element with respect to the center of mass of the corresponding rigid element and the angles $\Delta \varphi_i$, for the torsion relative to the orientation of the skeletal part. In three dimensions six coordinates are necessary, three for the displacement $\Delta x_i, \Delta y_i, \Delta z_i$, and three $\Delta \alpha_i, \Delta \beta_i, \Delta \gamma_i$ for the torsion. The motion of each wobbling mass is determined by the six (or three in the plane case) equations of motion for an extended body analogously to eqs. (3.1), (3.18a) and (3.20). The forces and torques acting in addition to gravity are given by the coupling mechanism between skeletal and wobbling part and depend on the displacement coordinates. Via *actio = reactio* the same forces and torques act on the skeletal part in the opposite direction.

Therefore, a multi-linked system with wobbling masses possesses the same number of internal torques reflecting the free will.

To adjust as well as possible the coupling between the skeletal part and the wobbling mass experimental input is necessary. In general, for a small displacement the coupling is very loose and it becomes stiff in a narrow range. Such a behaviour can be described by a dependence of the form (displacement)^m with an exponent $m \approx 3 \dots 4$. Furthermore, the motions of the wobbling masses are strongly damped and come to rest after some few oscillations. This is described by a dependence of the velocities on the displacements. Additionally, it must be taken into account that the coupling constants of the wobbling masses are different for displacements parallel or perpendicular to the skeletal parts. The relative torques of the angular displacements $\Delta\varphi_i$ can be treated in an analogous manner. After a long period of biomechanical experiments together with fitting procedures we have found that the following relations for the coupling forces seem to be (for the plane case) the best approximations in the framework of our modelling.

$$T_{wi} = a_{wi}\Delta\varphi_i + b_{wi}\dot{\Delta\varphi}_i \quad (4.3a)$$

$$F_{wi,l} = c_{wi,l}\text{sign}(\Delta r_{il})|\Delta r_{il}|^3 + d_{wi,l}\dot{\Delta r}_{il} \quad (4.3b)$$

$$F_{wi,t} = c_{wi,t}\text{sign}(\Delta r_{it})|\Delta r_{it}|^3 + d_{wi,t}\dot{\Delta r}_{it} \quad (4.3c)$$

The longitudinal and transversal components $F_{wi,l}$ and $F_{wi,t}$ of the coupling forces are then decomposed onto the space-fixed axes and yield the Cartesian components $F_{wi,x}$ and $F_{wi,z}$, which enter into the equations of motion. The coupling constants a_{wi} , b_{wi} , $c_{wi,l}$, $d_{wi,l}$, $c_{wi,t}$ and $d_{wi,t}$ must be adjusted individually.

To avoid confusion it should be stated that in the model presented here only the skeletal parts are connected by joints and, therefore, only they couple via the internal reaction forces, but each wobbling mass is only coupled to its corresponding skeletal part.

To become more concrete, we will discuss a three-linked wobbling mass model in detail and demonstrate some animation sequences.

4.3 The three-linked wobbling mass model

The minimum number of segments to simulate a human being is three: one segment for the trunk, a second for the two (parallel) thighs and a third for the two lower legs.

A wobbling mass element is coupled to each segment. Even this simplest model possesses $n + 2 + 3n = 4n + 2 = 14$ (for $n = 3$) coordinates (see Fig. 4.5) in the plane case and 14 second order differential equations must be integrated for the dynamic simulation. Furthermore, for an explicit calculation the geometrical and mechanical parameters of the model must be fixed.

4.3.1 Geometrical and mechanical parameters

As geometrical quantities we have the three lengths l_i of the segments

lower leg including foot $l_1 = 0.43$ m,

thigh $l_2 = 0.45$ m,

trunk including head $l_3 = 0.75$ m

and the biologically possible ranges of the two angles

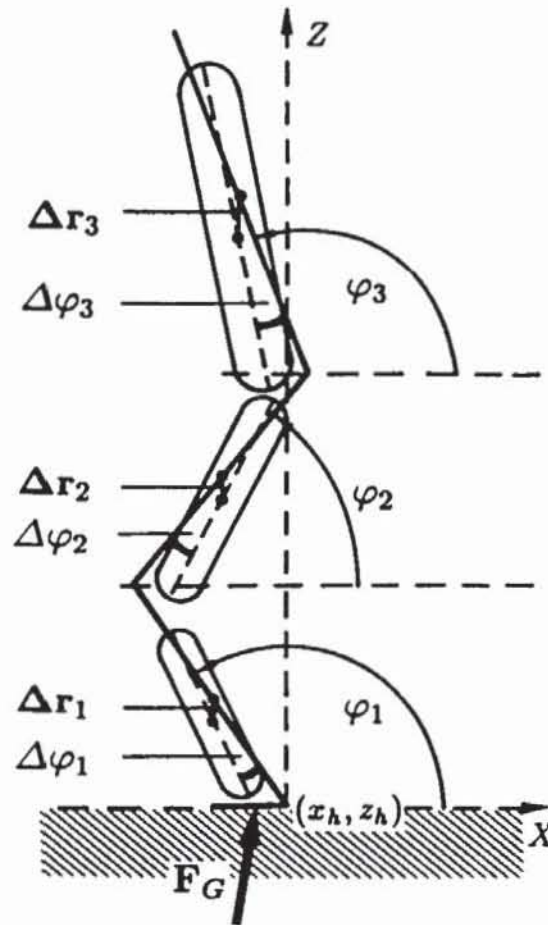


Fig. 4.5. Coordinates of the three-linked wobbling mass model. The position of the heel is described by the Cartesian coordinates (x_h, z_h) , the orientations of the skeletal segments by the angles $\varphi_1, \varphi_2, \varphi_3$ and the positions of the wobbling masses relative to their corresponding skeletal parts by the vectors of displacement and the angles of rotation (cf. Fig. 4.4).

$$15^\circ \leq \varphi_{\text{knee}} = 180^\circ - \varphi_2 + \varphi_1 \leq 182^\circ,$$

$$15^\circ \leq \varphi_{\text{hip}} = 180^\circ + \varphi_3 - \varphi_2 \leq 210^\circ.$$

The mechanical quantities of the model for each segment are the mass m_i , the disposition in a skeletal part with mass $m_{i,s}$ and a wobbling part $m_{i,w}$, and the corresponding moments of inertia $\Theta_{i,s}$ and $\Theta_{i,w}$. (The index s stands for *skeletal* and w for *wobbling*.)

The masses of the segments can be taken from the medical literature and are given in units of the total mass m :

mass of a lower leg including foot $m_1 = 0.06 m$,

mass of a thigh $m_2 = 0.11 m$,

mass of the trunk including head and arms $m_3 = 0.66 m$.

To obtain numbers for the percental disposition of each segment into a skeletal and wobbling part is much more difficult. Our experimental studies together with fitting procedures yield as reasonable percentages:

lower leg: skeletal part 25%, wobbling mass 75%,

thigh: skeletal part 25%, wobbling mass 75%,

trunk: skeletal part 50%, wobbling mass 50%.

Experimental data for the moments of inertia of the segments relative to their centers of mass although are not available in the literature, therefore, we approximately calculate these quantities by means of the relation for the moment of inertia of a cylinder with mass m_i , length l_i , and average radius r_i perpendicular to its axis

$$\theta_i = m_i \left(\frac{l_i^2}{12} + \frac{r_i^2}{4} \right) \quad (4.4)$$

Using the lengths l_i of the segments and experimentally determined radii we obtain from (4.4) the following values for the six moments of inertia divided by the total mass:

$$\begin{aligned} \theta_{1s}/m &= 0.00023 \text{ m}^2 & \theta_{1w}/m &= 0.00037 \text{ m}^2 \\ \theta_{2s}/m &= 0.00047 \text{ m}^2 & \theta_{2w}/m &= 0.00152 \text{ m}^2 \\ \theta_{3s}/m &= 0.00845 \text{ m}^2 & \theta_{3w}/m &= 0.03380 \text{ m}^2. \end{aligned}$$

4.3.2 Equations of motion

To obtain an impression of the form and complexity of the problem, in the following the equations of motion for the three-linked wobbling mass model using the coordinates from Fig. 4.5 are explicitly given (after a lengthy but elementary calculation):

$$\begin{aligned} m\ddot{x}_h &- (m_1 + 2m_2 + 2m_3) \frac{l_1}{2} \sin \varphi_1 \ddot{\varphi}_1 - (m_2 + 2m_3) \frac{l_2}{2} \sin \varphi_2 \ddot{\varphi}_2 \\ &- m_3 \frac{l_3}{2} \sin \varphi_3 \ddot{\varphi}_3 + m_{1w} \Delta \ddot{x}_1 + m_{2w} \Delta \ddot{x}_2 + m_{3w} \Delta \ddot{x}_3 \end{aligned} \quad (4.5a)$$

$$\begin{aligned} &= (m_1 + 2m_2 + 2m_3) \frac{l_1}{2} \cos \varphi_1 \dot{\varphi}_1^2 + (m_2 + 2m_3) \frac{l_2}{2} \cos \varphi_2 \dot{\varphi}_2^2 \\ &+ m_3 \frac{l_3}{2} \cos \varphi_3 \dot{\varphi}_3^2 + F_{Gz} \\ m\ddot{z}_h &+ (m_1 + 2m_2 + 2m_3) \frac{l_1}{2} \cos \varphi_1 \ddot{\varphi}_1 + (m_2 + 2m_3) \frac{l_2}{2} \cos \varphi_2 \ddot{\varphi}_2 \\ &+ m_3 \frac{l_3}{2} \cos \varphi_3 \ddot{\varphi}_3 + m_{1w} \Delta \ddot{z}_1 + m_{2w} \Delta \ddot{z}_2 + m_{3w} \Delta \ddot{z}_3 \end{aligned} \quad (4.5b)$$

$$\begin{aligned} &= (m_1 + 2m_2 + 2m_3) \frac{l_1}{2} \sin \varphi_1 \dot{\varphi}_1^2 + (m_2 + 2m_3) \frac{l_2}{2} \sin \varphi_2 \dot{\varphi}_2^2 \\ &+ m_3 \frac{l_3}{2} \sin \varphi_3 \dot{\varphi}_3^2 + F_{Gz} - mg \\ -\theta_{1s} \ddot{\varphi}_1 &+ m_{1s} \frac{l_1}{2} \sin \varphi_1 \Delta \ddot{x}_1 - m_{1s} \frac{l_1}{2} \cos \varphi_1 \Delta \ddot{z}_1 \\ &= T_G - \frac{l_1}{2} \sin \varphi_1 \left[F_{Gz} + \frac{m_1}{m_{1w}} F_{w1z} \right] \end{aligned} \quad (4.5c)$$

$$\begin{aligned} &+ \frac{l_1}{2} \cos \varphi_1 \left[F_{Gz} + \frac{m_1}{m_{1w}} F_{w1z} \right] + T_{12} - T_{w1} + T_{corr1} \\ -\theta_{2s} \ddot{\varphi}_2 &+ m_{1s} l_2 \sin \varphi_2 \Delta \ddot{x}_1 - m_{1s} l_2 \cos \varphi_2 \Delta \ddot{z}_1 \\ &+ m_{2s} \frac{l_2}{2} \sin \varphi_2 \Delta \ddot{x}_2 - m_{2s} \frac{l_2}{2} \cos \varphi_2 \Delta \ddot{z}_2 \end{aligned} \quad (4.5d)$$

$$\begin{aligned} &= -l_2 \sin \varphi_2 \left[F_{Gz} + \frac{m_1}{m_{1w}} F_{w1z} + \frac{1}{2} \frac{m_2}{m_{2w}} F_{w2z} \right] \\ &+ l_2 \cos \varphi_2 \left[F_{Gz} + \frac{m_1}{m_{1w}} F_{w1z} + \frac{1}{2} \frac{m_2}{m_{2w}} F_{w2z} \right] - T_{12} + T_{23} - T_{w2} + T_{corr2} \end{aligned}$$

$$\begin{aligned}
-\theta_{3w}\bar{\varphi}_3 - m_{3s}\frac{l_3}{2}\sin\varphi_3\Delta\bar{x}_3 + m_{3s}\frac{l_3}{2}\cos\varphi_3\Delta\bar{z}_3 \\
= \left[\frac{l_3}{2}\sin\varphi_3\frac{m_3}{m_{3w}}F_{w3x} - \frac{l_3}{2}\cos\varphi_3\frac{m_3}{m_{3w}}F_{w3z} \right] - T_{23} - T_{w3} + T_{corr3}
\end{aligned} \tag{4.5e}$$

$$\bar{x}_h - \frac{l_1}{2}\sin\varphi_1\bar{\varphi}_1 + \Delta\bar{x}_1 = \frac{l_1}{2}\cos\varphi_1\dot{\varphi}_1^2 - \frac{1}{m_{1w}}F_{w1x} \tag{4.5f}$$

$$\bar{z}_h + \frac{l_1}{2}\cos\varphi_1\bar{\varphi}_1 + \Delta\bar{z}_1 = \frac{l_1}{2}\sin\varphi_1\dot{\varphi}_1^2 - \frac{1}{m_{1w}}F_{w1z} - g \tag{4.5g}$$

$$\begin{aligned}
\bar{x}_h - l_1\sin\varphi_1\bar{\varphi}_1 - \frac{l_2}{2}\sin\varphi_2\bar{\varphi}_2 + \Delta\bar{x}_2 \\
= l_1\cos\varphi_1\dot{\varphi}_1^2 + \frac{l_2}{2}\cos\varphi_2\dot{\varphi}_2^2 - \frac{1}{m_{2w}}F_{w2x}
\end{aligned} \tag{4.5h}$$

$$\begin{aligned}
\bar{z}_h + l_1\cos\varphi_1\bar{\varphi}_1 + \frac{l_2}{2}\cos\varphi_2\bar{\varphi}_2 + \Delta\bar{z}_2 \\
= l_1\sin\varphi_1\dot{\varphi}_1^2 + \frac{l_2}{2}\sin\varphi_2\dot{\varphi}_2^2 - \frac{1}{m_{2w}}F_{w2z} - g
\end{aligned} \tag{4.5i}$$

$$\begin{aligned}
\bar{x}_h - l_1\sin\varphi_1\bar{\varphi}_1 - l_2\sin\varphi_2\bar{\varphi}_2 - \frac{l_3}{2}\sin\varphi_3\bar{\varphi}_3 + \Delta\bar{x}_3 \\
= l_1\cos\varphi_1\dot{\varphi}_1^2 + l_2\cos\varphi_2\dot{\varphi}_2^2 + \frac{l_3}{2}\cos\varphi_3\dot{\varphi}_3^2 - \frac{1}{m_{3w}}F_{w3x}
\end{aligned} \tag{4.5j}$$

$$\begin{aligned}
\bar{z}_h + l_1\cos\varphi_1\bar{\varphi}_1 + l_2\cos\varphi_2\bar{\varphi}_2 + \frac{l_3}{2}\cos\varphi_3\bar{\varphi}_3 + \Delta\bar{z}_3 \\
= l_1\sin\varphi_1\dot{\varphi}_1^2 + l_2\sin\varphi_2\dot{\varphi}_2^2 + \frac{l_3}{2}\sin\varphi_3\dot{\varphi}_3^2 - \frac{1}{m_{3w}}F_{w3z} - g
\end{aligned} \tag{4.5k}$$

$$-\theta_{1w}(\bar{\varphi}_1 + \Delta\bar{\varphi}_1) = T_{w1} \tag{4.5l}$$

$$-\theta_{2w}(\bar{\varphi}_2 + \Delta\bar{\varphi}_2) = T_{w2} \tag{4.5m}$$

$$-\theta_{3w}(\bar{\varphi}_3 + \Delta\bar{\varphi}_3) = T_{w3} \tag{4.5n}$$

In addition to the symbols already explained in the previous sections in Eq. (4.5) some further new quantities occur, namely the x - and z -component of the ground reaction force F_{Gx} and F_{Gz} , the torque T_G , which is transmitted at the foot by the ground reaction force (cf. Fig. 4.5) the torques T_{12}, T_{23} , which are generated by skeletal muscles in the knee and hip joints. T_{corr_i} is an additional torque in each joint, which is necessary to correct the violation of the angular momentum caused by the coupling of the wobbling mass. These latter quantities are tiny and only of theoretical interest.

It should be mentioned that the structure of the equations is always the same as in Eq. (4.5). This is valid for two and three dimensions and for an arbitrary number of segments. Denoting the vector of independent coordinates with \mathbf{x} , the mass matrix with \underline{M} , the vector of the generalized Coriolis and centrifugal forces with \underline{C} and the vector of the generalized forces and torques acting on each segment with \underline{F} the equations of motion can be generally written in the form

$$\underline{M}(\mathbf{x}) \cdot \ddot{\mathbf{x}} + \underline{C}(\mathbf{x}, \dot{\mathbf{x}}) = \underline{F}(\mathbf{x}, \dot{\mathbf{x}}) \quad , \tag{4.6}$$

to which standard integration routines can be applied.

4.4 Inverse and direct dynamics

The equations of motion can be considered from two basically different points of view. On the one hand the motion can be regarded as known, then the left hand sides of the equations are determined and the forces and torques on the right hand side can be calculated. This procedure requires experimental input either by film analysis or by measurements of accelerations. On the other hand with all external forces and internal torques given the integration of the equations of motion leads to the physically correct motion of the system. We will now discuss in some detail these two aspects.

4.4.1 Inverse dynamics

The simplest case is to fix markers at the body and to follow the space-time trajectory of these points with the help of a high-speed camera or other adequate systems. Ideally, as a result all coordinates describing the system are given on a discrete time grid with typical time steps of the order of milliseconds. In order to obtain the forces and torques these time sequences have to be differentiated twice (cf. Eq. (4.5) and (4.6)). This numerical differentiation leads to an artificially oscillating behaviour and to a reduced accuracy in the time resolution. An additional complication results from the fact that the markers are fixed at the skin which shows a displacement with respect to the skeleton especially by motions with high accelerations. However, for slow motions the method of film analysis works well and is successfully applied in gait analysis in biomechanical research (e.g. Aleshinsky and Zatsiorsky, 1978; Zajac and Gordon, 1989).

In order to experimentally investigate motions with high acceleration like impacts during contact with the ground we have developed an alternative method to determine the internal forces and torques. To avoid the problems introduced by the numerical differentiation the external forces are directly measured by means of force platforms and a sufficient number of accelerations by appropriately placed accelerometers. These devices can be operated at higher frequencies of about 4 kHz yielding experimental data with a far better time resolution. As follows from the general considerations in Sect. 4.1.1 concerning the degrees of freedom of a multi-linked model and as can be explicitly seen from Eq. (4.5) in the case of a plane three-linked model the two internal torques are unknown quantities even if all external forces and torques are measured. These two (or $n - 1$ in the general plane or $3(n - 1)$ in the most general three-dimensional case) internal torques are not accessible to a direct measurement without invasive operations. This problem can unbloodily be solved by measuring the corresponding number of accelerations. Then, the internal torques are gained from these experimental input not by twofold differentiating but by integrating the equations of motion, a procedure, which is numerically far more stable and yields a much higher degree of accuracy.

With the external and internal forces and torques at hand the physically correct continuous motion can be calculated in a reproducible way. Furthermore, at each arbitrary plane of intersection of the body the forces and torques transmitted in this plane can be determined at any moment, which is of special interest in biomechanical problems.

4.4.2 Controlling direct dynamics

The ultimate goal of producing animation sequences for human beings and animals is the physically realistic simulation of the motion taking into account the biomechanical constraints, the correct mechanical properties of the objects and a behaviour controlled feedback for the building up of the internal torques. This means that all forces and torques, which enter the equations of motion, are determined either by a relation between the force, the deformation and the deformation-velocity or by a self-controlling mechanism.

4.4.2.1 External reaction forces

These forces arise when a body segment collides with objects in its environment. For almost all possible situations a relation of the form

$$F = a (z_{\text{deform}})^b + d \dot{z}_{\text{deform}} \quad (4.7)$$

for each component of the force with appropriately adjusted parameters is a sufficiently good approximation. The parameters can be determined either empirically or in the frame of an elasto-mechanical theory. To give an example, in Fig. 4.6 the experimental force-deformation relation of the human heel is shown for the static and a dynamic case.

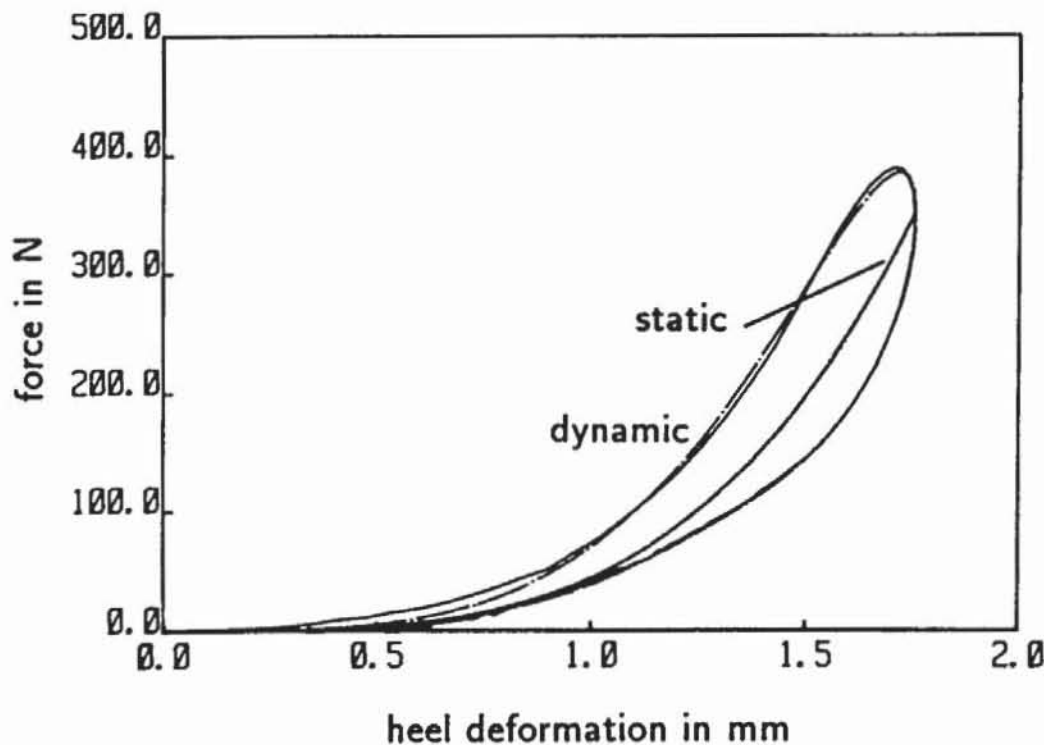


Fig. 4.6. Empirical force-deformation relation of the human heel for the static and a dynamic case.

In general, the relation for the reaction force is a superposition of the mechanical properties of the body and the object. An example is a down jump on a plank, where as well the elastic properties of the heel enter as the bending of the plank (cf. Sect. 4.5). In the presence of friction as a further constraint the component of the reaction force tangential to the striking surfaces must be smaller than the component perpendicular to the surface times the coefficient of friction otherwise sliding sets on.

4.4.2.2 Active internal torques

As discussed previously the internal torques produced by the muscles determine the controlled part of the motion. One way to find the torques for a desired motion as functions of time is the simple trial and error method, e.g. starting from a given initial state, varying the torques and integrating the equations of motion until the desired final state is achieved. A far more sophisticated way is to control the increase and the decrease of the internal torques by an active feedback mechanism. This method shall be demonstrated by the example of the active deceleration phase after a down jump.

During the free-fall phase the joint angles are assumed to be constant. Therefore, the internal net torques must be zero. Shortly after the impact the heels have come to rest, the velocity of the center of mass of the whole body is somewhat reduced by the impact and at the same time the bending of the body segments abruptly starts with definite angular velocities. They have to be stopped by building up the internal torques. Right before the impact the muscles are actively strained, however, without producing net torques. Caused by the bending of the segments the joint angles alter, the strained muscles and tendons are expanded and automatically produce torques, already a few milliseconds after impact. Due to the mechanical properties of the muscles and ligaments the increase of the torques is approximately proportional to the angular velocities $\dot{\varphi}_{ij}$ of the joint angles φ_{ij} . Therefore, in this start phase of increasing torques the internal torque T_{ij} in a joint at the time $t + dt$ can be calculated by

$$T_{ij}(t + dt) = T_{ij}(t) + c'_{ij}\dot{\varphi}_{ij}(t)dt \quad . \quad (4.8)$$

Of course, the torques cannot increase infinitely. Each joint is only able to build up a maximum torque T_{ij}^{\max} . Therefore, the increase of the torque will slow down when approaching this limiting torque. Such a behaviour can well be modelled by modifying (4.8) by an additional factor

$$T_{ij}(t + dt) = T_{ij}(t) + c_{ij}\dot{\varphi}_{ij}(t) \left(\frac{T_{ij}^{\max} - T_{ij}(t)}{T_{ij}^{\max}} \right) dt \quad . \quad (4.9)$$

Eq. (4.9) leads to a linear increase of the torque at the beginning and a smooth approaching to T_{ij}^{\max} . With appropriate chosen parameters for each joint the torque evolution of the form (4.9) leads, e.g. for a down jump, to a physically realistic hopping of the model.

To produce more and more complex motions more and more control parameters must be introduced in modelling the torques. The alteration of the torques can be controlled either by the coordinates and velocities of the body segments themselves or by external conditions of the environment. A simple example is the controlling of the deceleration phase after a down jump by the z -component of the velocity of the center of mass which can be written as an additional factor in (4.9) of the form

$$\begin{aligned} T_{ij}(t + dt) & \\ & = T_{ij}(t) + c_{ij}\dot{\varphi}_{ij}(t) \left(\frac{T_{ij}^{\max} - T_{ij}(t)}{T_{ij}^{\max}} \right) \cdot \left[1 + a_{ij} \left(\frac{\dot{z}_c}{\dot{z}_c^{\text{impact}}} - 1 \right) \right] dt \quad . \end{aligned} \quad (4.10)$$

The choice of the parameter a_{ij} determines at what squat position the body comes to rest.

As an example for the modelling quality which can be achieved within the framework presented, in Fig. 4.7 the measured ground reaction force of a down jump (cf.

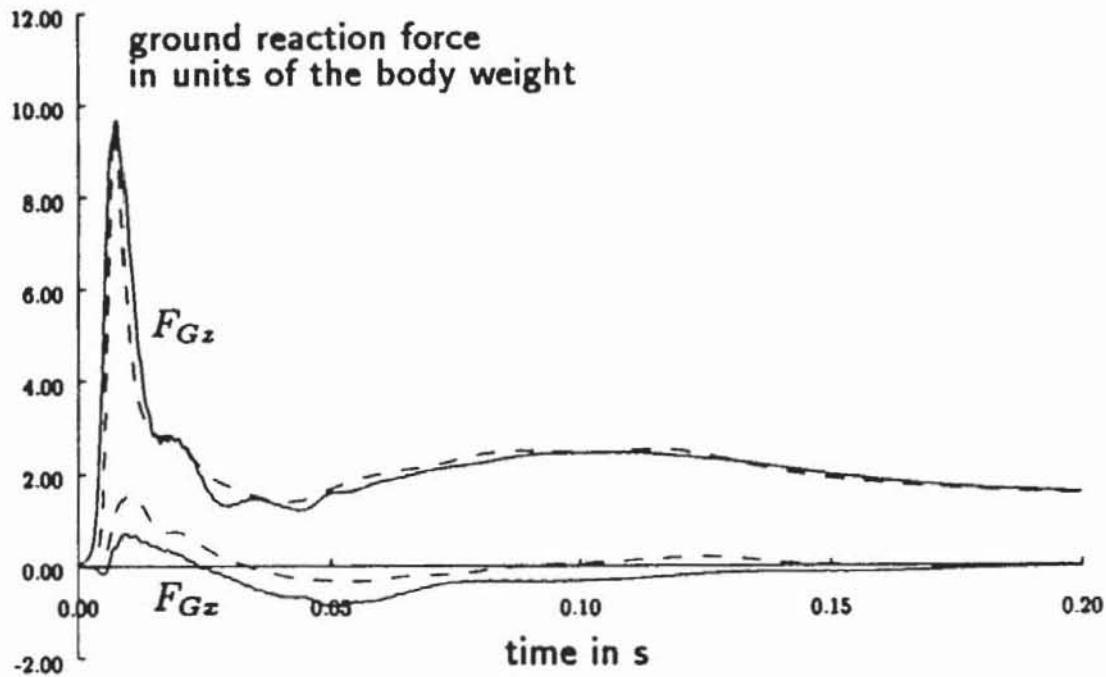


Fig. 4.7. Comparison of the measured and calculated components of the ground reaction forces during the landing on the heel and the following deceleration phase after a down jump. The theoretical curves are produced by integrating the equations of motion (4.5) without any experimental input.

Fig. 4.3) is shown together with the calculated force which was produced without any experimental input. This excellent agreement proves that the whole motion is physically correct described within an error of a few percents.

To remain realistic for actively motivated torques the finite reaction time of a human being, which is of the order of 0.1 s, must be taken into account. This means a retardation of this amount in using coordinates and velocities for the calculation of those changes in the torques which are caused by reactions of external conditions. Studies of such kind are also of great interest for biomechanical and behaviour research. At this stage modern methods of controlled learning must be applied. Besides these things a retardation is also not a trivial problem for the numerical treatment of the integration of the equations of motion.

4.5 Jumps and impacts

The best way to demonstrate the capabilities of our dynamic simulation are, of course, animation sequences. In the following Figs. 4.8 and 4.9 snapshots of two down jumps of an extended five-linked model are shown. In the first example the internal torques are controlled in such a way that the model comes to rest in a squat position and in the second example that the model jumps off again and performs a somersault.

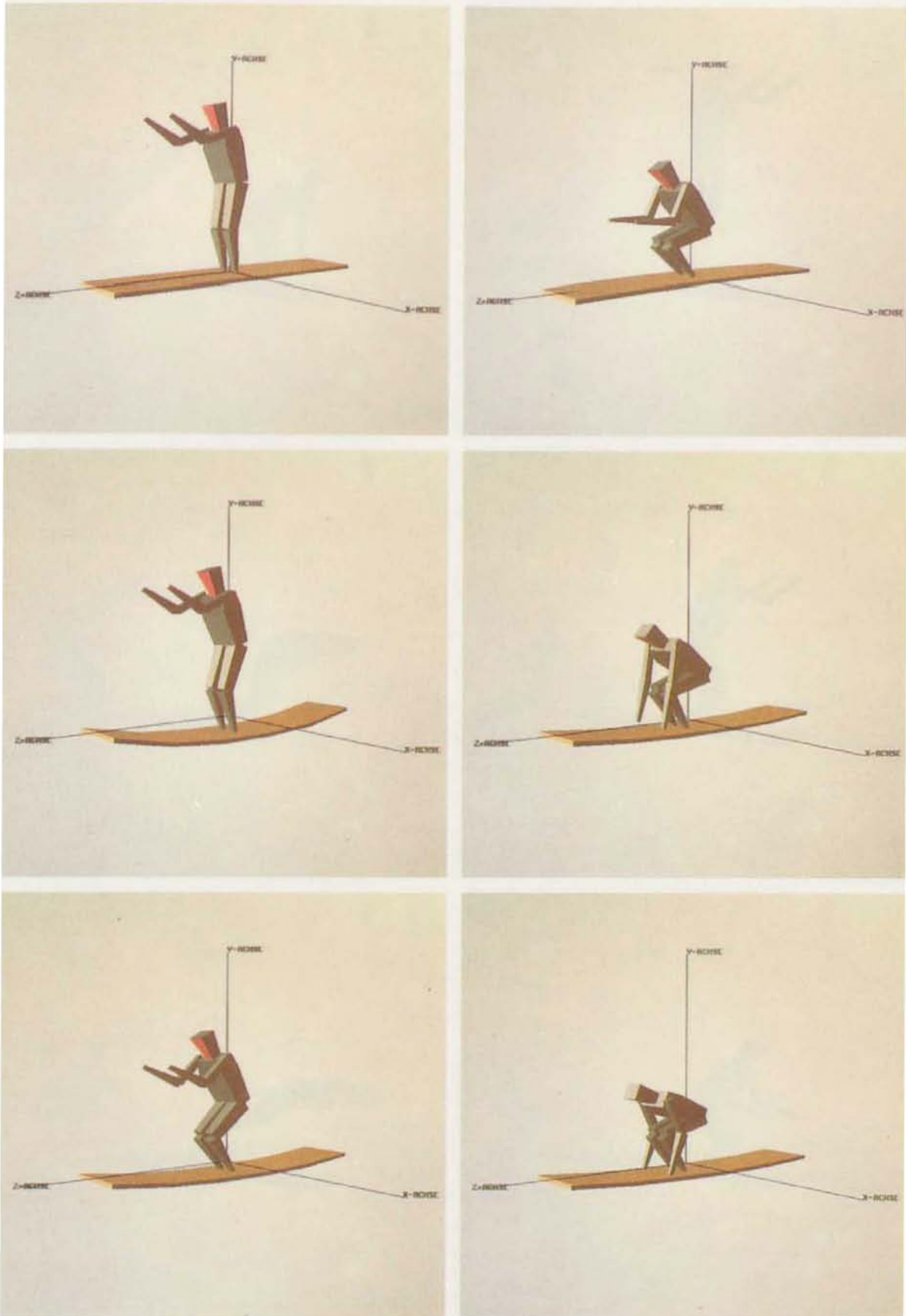


Fig. 4.8. Snapshots of a down jump of a five-linked model with landing on a bending plank. The internal torques are controlled in such a way that the model comes to rest in a squat position.

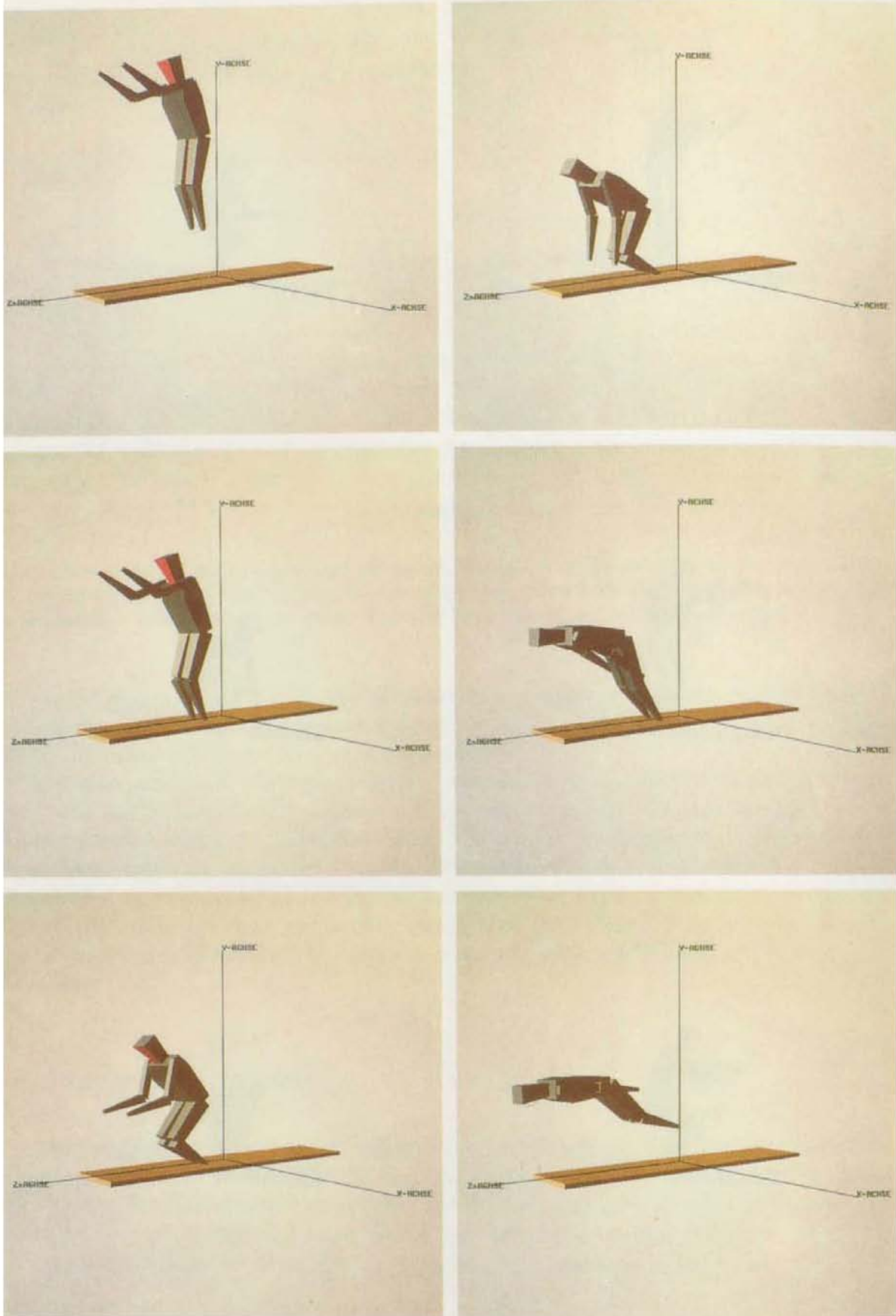


Fig. 4.9. Snapshots of a down jump of a five-linked model with landing on a stiff plank. The internal torques are here controlled in such a way that the model jumps off again and performs a somersault.

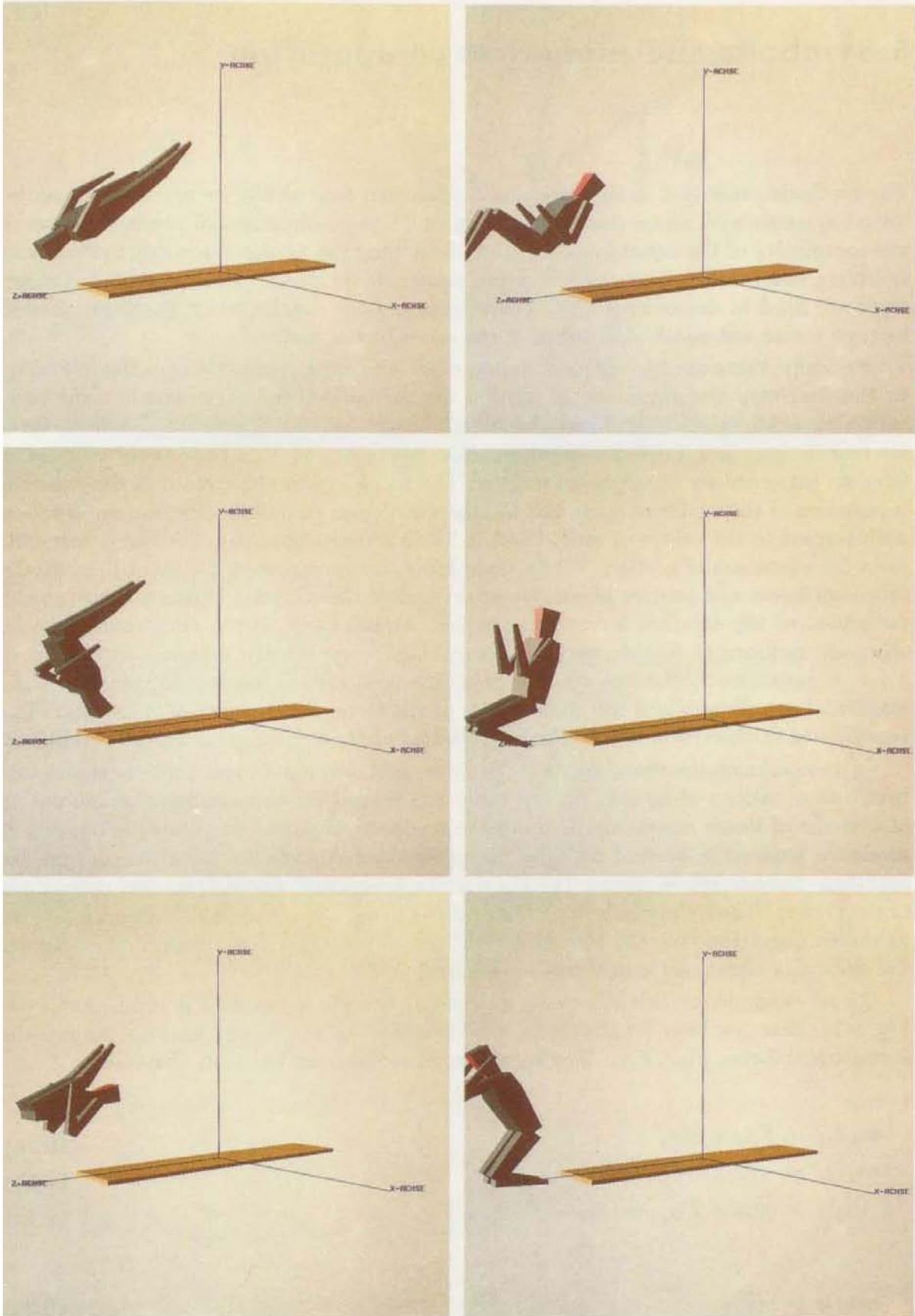


Fig. 4.9. (continued)

5 Symbolic and numerical computation

The methods presented in the previous chapter can canonically be extended to multi-linked systems with more than three links or to three-dimensional models. However, the complexity of the equations of motion describing the planar three-link system with wobbling mass makes it obvious that the equations for much more complicated structures are hard to derive manually. Therefore, symbolic manipulation packages need to be used for an automatic derivation of the equations of motion.

Basically, there are two different approaches: The most common one is the following. In the first step the equations of motion are formulated for every single rigid body assuming it to be unconstrained. Each rigid body has six degrees of freedom, three for translation, and three for rotation. Corresponding to this number of degrees of freedom there are six equations of motion: The three Newtonian equations describe the translation of the centre of mass and the three Eulerian equations describe the rotation with respect to the centre of mass (Sect. 3.2). In a multi-linked system the n segments yield $6n$ equations of motion. While assembling the segments to a system the initially unknown forces and torques of constraint that effect the coupling between the segments are added to the external forces and torques. Additionally, the m constraints give an adequate number of further equations resulting in an exactly determined system of $6n + m$ equations. Unknown quantities in this case are the second derivatives of the segmental coordinates and the components of the forces and torques of constraint. The coordinates themselves and their first derivatives are known from the initial conditions.

In a second step the components of the forces and torques of constraint are eliminated from the equations of motion by the usual procedures for the symbolic manipulation of systems of linear equations. If there are m constraints the number of equations of motion is reduced to a set of $6n - m$. Using these constraints all of the $6n$ coordinates and their derivatives are replaced by the $6n - m$ generalized coordinates and derivatives of the system. Thus, the whole procedure results in $6n - m$ equations containing $6n - m$ unknown quantities, i.e. the second derivatives of the generalized coordinates. Again, the system of equations is uniquely determined.

As an example for this approach we discuss the plane two-linked rigid model (cf. Fig. 5.1). Here, we have 8 unknowns, the 6 coordinates $x_{c1}, z_{c1}, \varphi_1, x_{c2}, z_{c2}, \varphi_2$ and the 2 constraint forces F_{12x}, F_{12z} . The equations of motion can be easily derived:

$$m_1 \ddot{x}_{c1} = F_{Gx} + F_{12x} \quad (5.1a)$$

$$m_1 \ddot{z}_{c1} = -m_1 g + F_{Gz} + F_{12z} \quad (5.1b)$$

$$\Theta_1 \ddot{\varphi}_1 = (\mathbf{r}_{11} \times \mathbf{F}_G)_y + (\mathbf{r}_{12} \times \mathbf{F}_{12})_y + T_{12} \quad (5.1c)$$

$$m_2 \ddot{x}_{c2} = -F_{12x} \quad (5.2a)$$

$$m_2 \ddot{z}_{c2} = -m_2 g - F_{12z} \quad (5.2b)$$

$$\Theta_2 \ddot{\varphi}_2 = (\mathbf{r}_{21} \times \mathbf{F}_{12})_y - T_{12} \quad (5.2c)$$

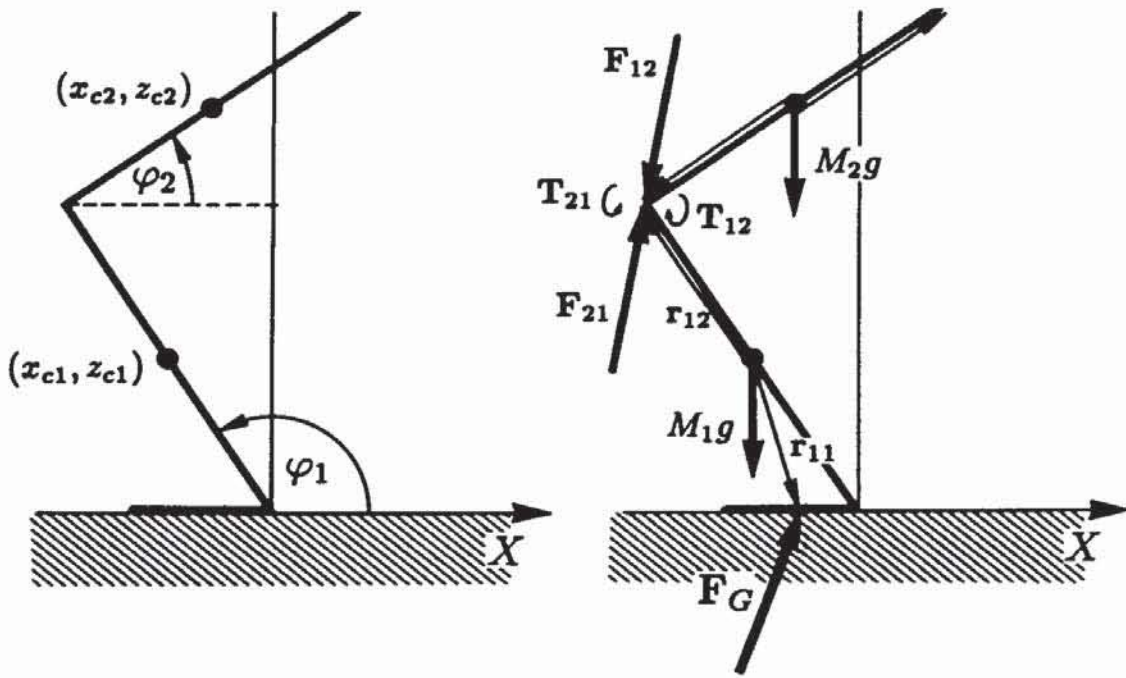


Fig. 5.1. The plane two-linked rigid model.

In addition, we have the joint conditions, which require that the upper end of the lower segment is connected to the lower end of the upper segment:

$$x_{c1} + \frac{l_1}{2} \cos \varphi_1 = x_{c2} - \frac{l_2}{2} \cos \varphi_2 \quad (5.3a)$$

$$z_{c1} + \frac{l_1}{2} \sin \varphi_1 = z_{c2} - \frac{l_2}{2} \sin \varphi_2 \quad (5.3b)$$

Using those, we can introduce 4 independent coordinates $x_h, z_h, \varphi_1, \varphi_2$ and eliminate the 2 unknown constraint forces and we get the minimum set of differential equations for 4 independent coordinates:

$$\begin{aligned} (m_1 + m_2)\ddot{x}_h - (m_1 + 2m_2)\frac{l_1}{2} \sin \varphi_1 \ddot{\varphi}_1 - m_2 \frac{l_2}{2} \sin \varphi_2 \ddot{\varphi}_2 \\ = (m_1 + 2m_2)\frac{l_1}{2} \cos \varphi_1 \dot{\varphi}_1^2 + m_2 \frac{l_2}{2} \cos \varphi_2 \dot{\varphi}_2^2 + F_{Gx} \end{aligned} \quad (5.4a)$$

$$\begin{aligned} m\ddot{z}_h + (m_1 + 2m_2)\frac{l_1}{2} \cos \varphi_1 \ddot{\varphi}_1 + m_2 \frac{l_2}{2} \cos \varphi_2 \ddot{\varphi}_2 \\ = (m_1 + 2m_2)\frac{l_1}{2} \sin \varphi_1 \dot{\varphi}_1^2 + m_2 \frac{l_2}{2} \sin \varphi_2 \dot{\varphi}_2^2 + F_{Gz} - mg \end{aligned} \quad (5.4b)$$

$$-\Theta_1 \ddot{\varphi}_1 = T_G - \frac{l_1}{2} \sin \varphi_1 F_{Gx} + \frac{l_1}{2} \cos \varphi_1 F_{Gz} + T_{12} \quad (5.5a)$$

$$-\Theta_2 \ddot{\varphi}_2 = -l_2 \sin \varphi_2 F_{Gx} + l_2 \cos \varphi_2 F_{Gz} - T_{12} \quad (5.5b)$$

However, serious problems occur when manipulating the equations symbolically following the course of this procedure. Huge algebraic terms are produced during the symbolic elimination of the forces and torques of constraint and the replacement of the

segmental coordinates by generalized coordinates. With an increasing number of degrees of freedom the size of these terms exceeds the capabilities of symbolic manipulation programs. Also, the generated source code may reach dimensions which are very hard to handle.

These problems can be avoided by utilizing a method, that requires the solution of a system of more equations, but whose terms are of a much simpler structure. The first step is the same as the one, described at the top of this section. The resulting system of linear equations at the end of this step, however, consists of $6n + m$ equations instead of $6n - m$. At this point the unknown quantities are the $6n$ second derivatives of the segmental coordinates and the m components of the forces and torques of constraint. It is possible to solve the system already at this stage and one obtains the second derivatives of the segmental coordinates and additionally the components of the forces and moments of constraint.

Using this method there are $6n$ differential equations of second order to be integrated instead of the $6n - m$ ones of the first approach. Moreover, at every integration step now there has to be solved a $6n + m$ system of linear equations compared to a $6n - m$ system. The particular terms of the equations, however, are quite simple and therefore easy to be generated automatically. Despite an increased number of equations the cpu-time needed for the second approach may decrease because of the highly simplified terms.

If we use this approach for the plane two-linked rigid model, we first have to differentiate the constraint conditions twice:

$$\ddot{x}_{c1} - \frac{l_1}{2}(\cos \varphi_1 \dot{\varphi}_1^2 + \sin \varphi_1 \ddot{\varphi}_1) = \ddot{x}_{c2} - \frac{l_2}{2}(\cos \varphi_2 \dot{\varphi}_2^2 + \sin \varphi_2 \ddot{\varphi}_2) \quad (5.6a)$$

$$\ddot{z}_{c1} + \frac{l_1}{2}(-\sin \varphi_1 \dot{\varphi}_1^2 + \cos \varphi_1 \ddot{\varphi}_1) = \ddot{z}_{c2} + \frac{l_2}{2}(-\sin \varphi_2 \dot{\varphi}_2^2 + \cos \varphi_2 \ddot{\varphi}_2) \quad (5.6b)$$

Together with eq. 5.1, we now have 8 linear equations for 6 second derivatives of the coordinates \ddot{x}_{c1} , \ddot{z}_{c1} , $\ddot{\varphi}_1$, \ddot{x}_{c2} , \ddot{z}_{c2} , $\ddot{\varphi}_2$ and 2 constraint forces F_{12x} , F_{12z} which have a much more simple structure than the minimum number eqs. 5.3 and 5.4.

Once, the equations of motion are derived in the general form of Eq. 4.6, they have to be integrated numerically. The first step in order to use one of the existing integration procedures is to split each of the second order equations into two first order equations by introducing a new independent variable. Preferably, the symbolic package already does this for you, before the equations are output in a form which can be easily integrated into the source code of your favourite programming language.

According to the forward formulation of the dynamic simulation the numerical problem can be characterized as an initial-value problem for a system of coupled ordinary differential equations:

$$\dot{\mathbf{x}} = \mathbf{f}(t, \mathbf{x}) \quad , \quad \mathbf{x}(t_0) = \mathbf{f}_0 \quad (5.7)$$

There are many excellent integration routines for initial-value problems available (for an overview of the area see Press, 1986) and one should definitely not start with implementing the Runge-Kutta algorithm again. For a good tradeoff between accuracy and efficiency a variable order, variable stepsize method should be chosen. We made good experiences with a code called DE (Shampine and Gordon, 1975), which is based on an Adams-Bashford predictor-corrector method. Especially when trying to resolve very sharp impacts the equations tend to appear stiff. This is a result of the predictor step which obviously cannot predict the correct behaviour after the impact. For this case, implicit BDF-methods (Gear, 1968) can be used.

The difference between eq. 4.6 and eq. 5.7 shows that the mass matrix has to be inverted for each evaluation of the right hand side. We use a routine from LINPACK for this part, but any other matrix solver will probably do the job. In order to reduce execution time an algorithm was suggested where it is not necessary to invert the mass matrix for each evaluation of the right hand side, but only, if it resulted in a significant change.

In the last chapter we tried to show that in our view the only reasonable way to reach a set of given end conditions (positions and velocities in the next keyframe) is to do a direct dynamic simulation with behavioural control through feedback from vision or other senses. However, there is still much more research to be done before this method will become computationally feasible. Until then, there is a need for being able to compute backwards. For a simple rigid body (like the rod from Sect. 3.3) this leads to a boundary-value problem. Numerical methods which can be used for this are either shooting algorithms or relaxation methods. We used extensively a relaxation procedure called Hemodes (Nobili and Turolla, 1988) which is based on the Henyey method (Henyey et al., 1964). For multi-linked models there is no unique solution for the boundary value problem. Solutions can only be found by optimizing additional constraints like form stability etc.

Once the dynamic behaviour of the skeleton is computed, there is much more to be done in order to generate a realistic looking human body, like the animation of the body surface and its reaction to deformations, hair, skin, and facial expressions, but all this is far beyond the scope of this tutorial.

6 A survey of commonly used computer animation approaches

Numerous articles on computer animation can be found in the proceedings of the SIGGRAPH conferences and in the proceedings of the Computer Animation Workshops. A survey of the state of the art in synthetic actors and motion control was given by Thalmann (1989) and Magnenat-Thalmann (1990). This chapter tries to relate some of the work done by other authors in the field of kinematic and dynamic animation to the concepts presented in this tutorial and defines some of the commonly used notions.

Usually, the basic structure for a human animation is a skeleton consisting of a connected set of rigid segments, corresponding to the limbs with joints at each intersection of the limbs. The animation of the skeleton is therefore determined by one position and all of the joint angles. The *direct kinematic* problem consists in computing the positions of the ends of the segments as a function of time while not taking into account the forces or the moments that cause the motion. This can be done without problems since the transformations from joint angles and angular velocities to Cartesian coordinates and velocities of the end points of the limbs are well behaved.

This is not true for the reverse transformation which is needed in *inverse kinematics* (Featherstone, 1983). Here, the animator is allowed to specify the desired end point positions and the sequence of joint angles is computed automatically. However, several special arrangements of the joint axes have been suggested for which closed form solu-

tions exist (Badler et al., 1985; Forsey and Wilhelms, 1988). In addition, the animator is required to impose internal constraints in order to obtain a unique orientation of the body. A system which allows to specify only one constraint at a time is not a very efficient way to solve. Therefore, iterative algorithms for satisfying multiple constraints according to a priority scheme in inverse kinematics were developed (Badler et al., 1987).

The problem with kinematic motion specification is how to determine a sequence of positions that result in a realistic looking animation. The basic alternatives are either getting the data from real world experiments (like film analysis) or finding them by trial and error, which both can be very tedious and therefore unacceptable in certain situations. The use of dynamic simulation avoids these limitations at a much higher cost and complexity of computation.

The major advantage of dynamics is, that given the time sequence of controlling torques and forces the predicted motion is accurate for the specified conditions and it would occur under these conditions in the real world. This means that the result of a dynamic simulation can be used as a basis for a perfect animation automatically taking into account the reaction to internal and external constraints like fields, collisions, torques and forces. Dynamical analysis couples the field of computer animation with research in the area of robotics, biomechanics and sports.

Like in kinematics, a direct and an inverse formulation can be stated. The *direct dynamics problem* consists of finding the trajectories of the end-point positions of the skeleton with regard to the forces and torques that describe the motion, whereas in *inverse dynamics* one looks for the forces and torques that produce a predefined motion. Inverse dynamics is mainly used for motion analysis, verification of direct dynamic simulations by comparison with experimental data or computing forces and torques for steering manipulators. The goal of animation, however, the production of movement, can only be reached with a direct dynamic simulation.

Numerous papers have been published during the last couple of years dealing with various aspects of the dynamic simulation. Wilhelms and Barsky (1985) have used the Gibbs-Appell formulation instead of Newton's law resulting in an algorithm with computational cost $O(n^4)$ where n is the number of joints. Armstrong and Green (1985) proposed a method which reduces the computational cost to $O(n)$ for the special case of tree-like skeletons, where rotation about the principal axes can be neglected. Kunii and Sun (1990) achieve a similar performance by deriving typical forces and torques for human movement from a database and by moving each segment unlinked from the others. They have to introduce another step of inverse dynamics in order to meet the constraints at the joints. A complete modelling system based on dynamic constraints was presented by Barzel and Barr (1988). They also use inverse dynamics to find the constraint forces which are necessary for the bodies in order to assemble themselves in accordance with the given constraints. Arnaldi et al. (1989) present a motion control system where the animation of a hand writing a letter was achieved with a combination of kinematic and dynamic motion control. Selbie (1989) reproduced a film recording of a running stride by getting the forces and torques from the experiment with inverse dynamics and using those in the forward dynamic simulation. The use of experimental data is quite common for producing realistic looking animation of walking, which is still based on motion analysis and heuristic models (Boulic et al., 1990).

More and more attention is paid to the control of the behaviour of dynamic simulations. With task level control, the animator specifies the broad outlines of a particular movement and the animation system fills in the details. This normally leads to an inverse kinematic or dynamic formulation of the problem with given constraints. Since there are many physical realistic alternatives for generating the in-between-motion, several opti-

mization strategies were developed (Witkin and Kass, 1988; Girad, 1987). An alternative approach, which is much more adapted to forward dynamic simulation is behavioural animation. Here, the motion of an object is generated according to rules which define how the objects react to their environment. This automatic stimulus-response mechanism removes the burden of a detailed motion specification from the animator and leads to realistic behaviour. Reynolds (1987) introduced this method when studying the problem of group trajectories for bird flocks and fish schools. The concept is essentially a particle simulation like the one presented in Sect. 3.2, where the particle interaction is set up in such a way, that they do not come too close together, but do not spread too far apart. Particle animation was also used by Sims (1990) when computing images of waterfalls, snow storms and fire. If the particle interaction can not be defined as clearly as in the previous examples, the behaviour has to be learned. Wilhelms (1990) has described an interactive network for solving a path finding problem.

References

- S.Y. Aleshinsky, V.M. Zatsiorsky: *J. Biomech.* **11** p. 101-108 (1978)
 W.W. Armstrong, M.W. Green: *The Visual Computer* **1**, 4 (1985)
 B. Arnaldi et al.: In *Proc. Computer Animation '89* p. 113-124
 N.I. Badler et al.: *The Visual Computer* **1**, 4 (1985)
 N.I. Badler et al.: *IEEE CG&A* **7** (1987)
 R. Barzel, A.H. Barr: *Computer Graphics* **22**, 4 (1988)
 R. Boulic et al.: In *Proc. Computer Animation '90* p. 61-80
 T. Ertl et al.: *Informationstechnologie* **33**, 2 (1991)
 R. Featherstone: *Int. J. of Robotics Research* **2**, 2 (1983)
 D. Forsey, J.P. Wilhelms: In *Proc. Graphics Interface '88* p. 8-15
 C.W. Gear: *Communications of the ACM* **14**, 176 (1968)
 M. Girad: *IEEE CG&A* **7**, 6 (1987)
 K. Gruber, J. Denoth, E. Stüssi, H. Ruder: In *International Series on Biomechanics 6B* p. 1095-1099 (1987)
 K. Gruber, J. Denoth, H. Ruder, E. Stüssi: *Z. Orthop.* **129**, 3 (1991)
 L.G. Henyey, J.E. Forbes, N.L. Gould: *Astrophysical Journal* **139**, 306 (1964)
 T.L. Kunii, L. Sun: In *CG International '90* p. 3-16
 N. Magnenat-Thalmann: In *CG International '90* p. 17-36
 L. Nobili, R. Turolla: *Astrophysical Journal* **333**, 248 (1988)
 W. Press: *Numerical Recipes*, Cambridge University Press (1986)
 H. Ruder et al.: In *Supercomputer '90* p. 67-82
 C. Reynolds: *Computer Graphics* **21**, 4 (1987)
 L.F. Shampine, M.K. Gordon: *Computer Solutions of Ordinary Differential Equations*, Freeman, San Francisco (1975)
 S. Selbie: In *Proc. Computer Animation '89* p. 33-45
 K. Sims: *Computer Graphics* **24**, 4 (1990)
 D. Thalmann: In *Proc. Computer Animation '89* p. 3-18
 J.P. Wilhelms: In *Proc. Computer Animation '90* p. 95-106
 J.P. Wilhelms, B.A. Barsky: In *Proc. Graphics Interface '85* p. 197-204
 A. Witkin, M. Kass: *Computer Graphics* **22**, 4 (1988)
 F.E. Zajac, M.E. Gordon: *Exercise and sport sciences reviews* **17** p. 187-230 (1989)